

AD-A102 993

ORINCON CORP. LA JOLLA CA
SIGNAL PROCESSING FOR SEISMIC SURVEILLANCE. (U)

F/0 8/11

JUL 81 H W SORENSEN

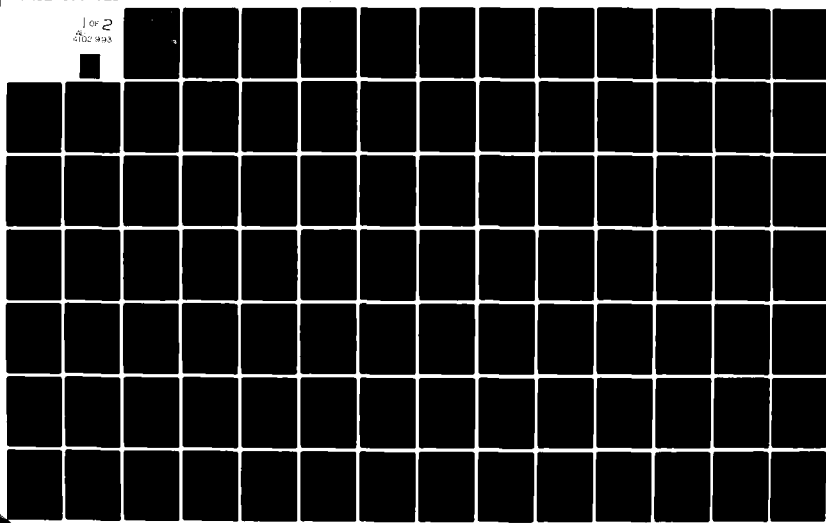
N00014-79-C-0390

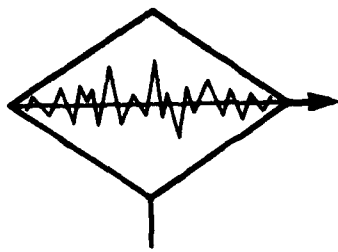
UNCLASSIFIED

OC-R-81-3090-2

NL

1 of 2
4102 993





ORINCON Corporation
LEVEL

1 - *12_Bs*

AD A102993



One file copy

[Signature]

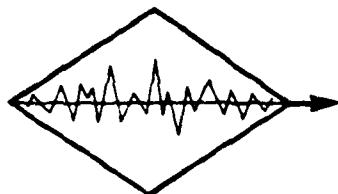


Operations

Research

817 30003
INformation CONtrol

DISTRIBUTION STATEMENT A
Approved for public release:
Distribution Unlimited



cont 46?
NR-08-327

12

ORINCON Corporation

3366 No. Torrey Pines Ct., Suite 320, La Jolla, CA 92037 (714) 455-5530

OC-R-81-3090-2

July 1981

SIGNAL PROCESSING FOR SEISMIC SURVEILLANCE

Final Technical Report

Contract No. N00014-79-C-~~3090~~

new
0390

DTIC 100-14000
SIGNAL PROCESSING FOR SEISMIC SURVEILLANCE
Final Technical Report
Contract No. N00014-79-C-~~3090~~
new
0390
JULY 1981
1981-14

Prepared by:

Harold W. Sorenson
Harold W. Sorenson
Principal Investigator

Approved by:

John T. Rickard
John T. Rickard
Program Manager

Submitted to:

Office of Naval Research
Department of the Navy
800 No. Quincy St.
Arlington, VA. 22217

DISTRIBUTION STATEMENT A
Approved for public release;
Distribution Unlimited

Operations

Research

INformation

CONtrol

TABLE OF CONTENTS

<u>Section</u>	<u>Title</u>	<u>Page</u>
ABSTRACT		1
INTRODUCTION AND OVERVIEW		2
PART I: BASIC PHYSICAL CONSIDERATIONS		8
I.1 General Description of the Sensors		9
I.2 Basic Modeling Assumptions		11
I.3 Basic Wave Characteristics		13
I.3.1 Compressional Waves		14
I.3.2 Shear Waves		17
I.3.3 Rayleigh Waves		18
I.3.4 Love Waves		20
I.4 Propagation Paths		21
I.4.1 Direct Waves		21
I.4.2 Reflected Waves		22
I.4.3 Refracted Waves		24
I.5 Error Sources		27
I.5.1 The Low Velocity Layer (LVL)		27
I.5.2 Dipping Layers		28
I.5.3 Diffractions		28
I.5.4 Noise Sources		29
I.6 Some Basic Modeling Considerations		31
PART II: GENERAL SIGNAL PROCESSING CONSIDERATIONS		36
II.1 Mathematical Models and Problem Definitions		37
II.1.1 The General Problem		37
II.1.2 Signals Generated by Seismic Waves		40
II.2 Some Array Processing Fundamentals		46
II.2.1 Response of a Beam-formed Array		48
II.2.2 Linear Array Response		50

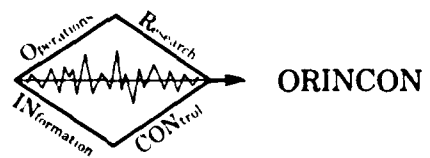
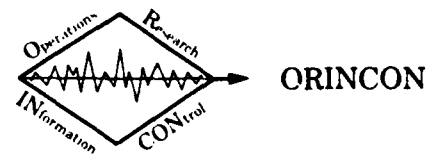
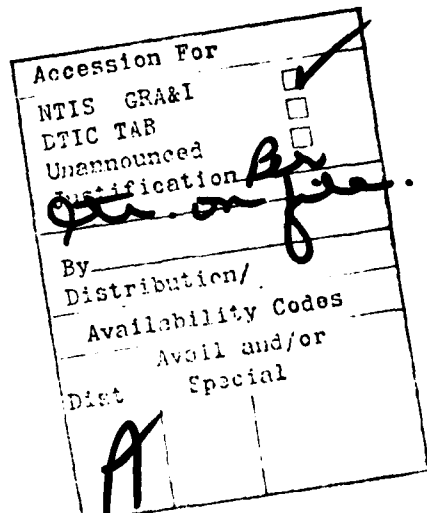


TABLE OF CONTENTS (Concluded)

<u>Section</u>	<u>Title</u>	<u>Page</u>
II.3	The Array Processing Problem and Array Directivity	58
II.3.1	The General Array Pattern	60
II.3.2	Optimal Array Directivity.....	63
II.3.3	Null Placement and Maximum Directivity ...	68
II.4	A Statistical Approach to Optimal Array Processing	71
II.4.1	The Linear, Minimum Mean-Square Error Estimator	73
II.4.2	The Maximum Likelihood Estimator and Adaptive Arrays	77
II.4.3	The Signal Detection Problem	81
II.4.4	The Effect of Signal Models	84
PART III: GENERAL ALGORITHMS AND RECOMMENDATIONS		89
III.1	General Algorithmic Considerations	90
III.2	Structure of the General Algorithms	94
III.3	Recommendations and Summary	109
REFERENCES		111

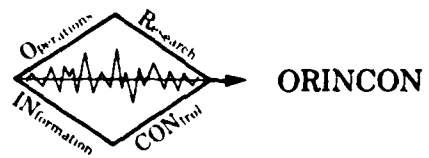


LIST OF FIGURES

<u>Figure</u>	<u>Caption</u>	<u>Page</u>
I.6-1	(p. 112) from Grant and West [2]	34
III-1	$A(n_x, n_y)$ for a linear array. $N = 7$; $w_i = 1$, $i = 1, 2, \dots, 7$	101
III-2	$A(n_x, n_y)$ for a circular array. $N = 7$, $w_i = 1$, $i = 1, 2, \dots, 10$	103
III-3	Azimuth and elevation angles for interference wave ...	105

LIST OF TABLES

<u>Table</u>	<u>Caption</u>	<u>Page</u>
I.3-1	(Telford et. al. [4]) $\alpha = 0.25$ dB/wavelength, $V = 2000$ m/sec	16

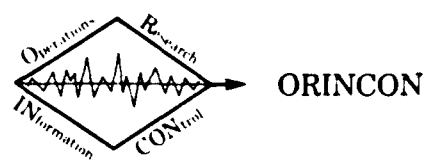


ABSTRACT

The objective in preparing this report is to provide a perspective on the signal processing problem that must be solved in order to produce a useful seismic surveillance system. The point-of-view is taken that the problem is nontrivial, thereby requiring a particularly careful development of the signal processing algorithms. The surveillance system is faced with the problem of detecting weak signals in the presence of incoherent and coherent noise sources. The signals that are sought generally have an unknown structure except for some important qualitative characteristics. These qualitative characteristics are identified by considering the propagation of seismic energy in terms of the possible wave types, propagation paths, and frequency ranges of possible signals.

The presentation is composed of three major sections. In Part I, basic physical considerations regarding the propagation and sensing of seismic energy are reviewed. This discussion provides physical motivation for the development of suitable signal processing algorithms. The general signal processing problem is defined in Part II. Array processing is reviewed and fundamental concepts are introduced in this section. General array processing algorithms are presented in Part III. The presentation in this section is intentionally brief as the algorithms are motivated and developed in Parts I and II.

The statement of the algorithms in Part III is very general. It is the contention of this report that the surveillance problem is sufficiently difficult that unnecessary haste must be avoided in developing specific algorithms of limited scope. It is important that a maximal amount of information is extracted from the sensor outputs in order to achieve desirable performance goals. Thus, the general structure of the algorithms is defined to serve as a basis for the evolution of specific algorithms that can be implemented in the seismic surveillance system. By proceeding early in the development to specific algorithms based upon restrictive assumptions, one can be misled in assessing the potential performance of the system.

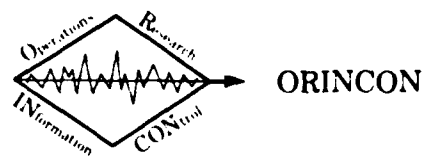


INTRODUCTION AND OVERVIEW

A primary objective of the signal processor is to detect seismic energy from an unknown source and to estimate the location of the source. Many sources are typified as introducing an impulse-like signal into the earth (e.g., an artillery recoil or a shell blast). Thus, the input signal occurs during a relatively short time interval. Because of the short time duration, the signal will contain a broad range of frequencies. Alternative sources of energy are provided by moving targets (e.g., tanks, trucks, aircraft). These sources introduce energy into the earth over longer time intervals and generally can be expected to define signals having narrowband characteristics. Both types of sources are considered in the following discussion.

The earth can be regarded as a channel that transmits the seismic energy generated by a source to sensors that provide information for the signal processor. The effect of the earth upon the input signal is very complex. A single source can generate several signals that may be observed by the sensors. These signals represent the different types of waves that can propagate in an elastic medium or the different propagation paths that are possible for a specific type of wave. To design the signal processor, the characteristics of the wave motion and the possible propagation paths must be understood and modeled.

The designer of the signal processor must be concerned with the properties of the signals received by the sensors. Because of the complex nature of the transmission channel, the signal received by the sensors is substantially different from the input signal generated by the source. To reduce the effects of the channel, the "sensor" typically consists of an array of three-axis geophones whose outputs are combined in an appropriate manner by the signal processor. The algorithms that define the processor must consider the following aspects.



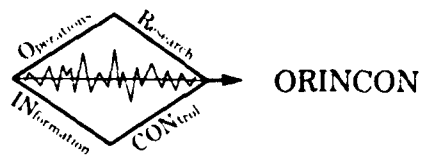
Signal Bandwidth: The range of frequencies which the signal is expected to contain must be established. As the bandwidth increases, the time duration of the signal diminishes.

Signal Power: The difficulty of the detection problem increases as the signal-to-noise ratio decreases. The signal power diminishes as the distance between the source and the sensor increases. Because the surveillance system is intended to operate at relatively long range (i.e., 10 to 20 km), the signal processor must be designed to operate at low signal-to-noise ratios (SNR).

Basic Wave Properties: Different types of waves induce different particle motions and these characteristics may be detected by a three-axis geophone. Then, the type of wave can be established. Because different waves propagate with different speeds, this classifications can be used in the signal processor to enhance detection and to aid in source localization.

Signals that are received by the sensor can result from waves that propagate along a variety of paths from the source to the sensor. Characterization of the propagation path is useful for several reasons. For example, a multiple reflection can arrive at a time that is sufficiently later than other arrivals that it appears to be a new signal. Thus, the detector may introduce a false alarm that can be otherwise avoided.

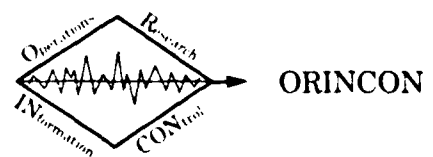
Wavefront Characteristics: Arrays of geophones must be used in order to obtain an increase in the effective SNR relative to a single geophone. But the geometrical separation of the elements of an array can introduce the requirement for characterizing the properties of the wavefront that is sensed by the geophones. Planar or spherical wavefronts may describe the propagation of many waves. However, in some circumstances the waves can exhibit a substantial distortion of the wavefront that must be considered by the signal processor, particularly for inter-array processing.



Error Sources: The analysis of wave propagation in the earth begins with several idealized assumptions. These assumptions lead to the general descriptions of signal bandwidth, signal power characteristics, wave properties, and wavefront behavior mentioned above. Deviations from the basic assumptions will introduce errors in the general models and the designer of the signal processor must be sensitive to effects of the potential error sources. These include effects such as dips in the layering of the earth, the influence of the weathered layer at the surface of the earth, elevation differences between the source and the sensor, and the irregularities in the subsurface composition.

The signal processing concerns that have been mentioned are addressed by defining idealized properties for the earth, developing mathematical models from these assumptions, and analyzing the consequences of the models. In Part I the assumptions and their consequences are reviewed to obtain the basic features that must be considered in the design of the signal processing algorithms. In Section I.2, the basic assumptions are stated and the models are reviewed. The types of waves and their general characteristics are discussed in Section I.3. The potential propagation paths are described in Section I.4. Some basic errors, sources and their effects are investigated in Section I.5.

Before beginning the discussion of the properties of the transmission channel, a general description of the sensors is provided in Section I.1. This discussion is intended to be qualitative and to establish a motivation for the subsequent description of the signal characteristics presented in Sections I.2 through I.5. The comments of Sections I.1 through I.5 are summarized in Section I.6. In this concluding section, some basic modeling and signal processing conclusions are stated and discussed.

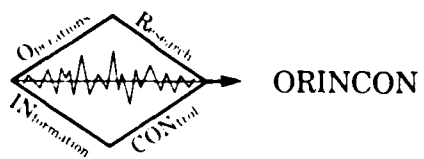


The analysis of the propagation of seismic energy leads to the identification of several wave types and a variety of propagation paths. Each wave induces a distinctive particle motion that must be measured by the sensors of the seismic surveillance system. Each wave travels with some average velocity and may be attenuated and dispersed along its path. These and other considerations lead to the conclusion that the signal received by a geophone from a particular seismic event will be a composite of different wave types that have traveled along several propagation paths. Consequently, the signal can be expected to have a very complicated and, largely, unpredictable character.

While the form of a signal must be regarded as unpredictable, some general characteristics can be assumed. For an impulsive source (e.g., an artillery recoil or a shell blast), the wave duration will be relatively brief, lasting for at most a few seconds so that a broad band signal is received. Geophysical considerations imply that detectable power is restricted to frequencies ranging from a few hertz to 100 hertz. The upper limit of the frequency band generally diminishes as the distance from the source to the sensor increases. The short-time duration of the signals induced by impulse-like sources suggests the need for time-domain rather than frequency-domain processing.

Other target sources can induce narrowband signals. For example, truck or tank motion imparts a persistent input to the earth that one would expect to have a narrowband characterization. For narrowband signals, frequency-domain processing is appropriate. These observations indicate that care must be taken in the signal processing to recognize the type of signal that is sought and to apply appropriate processing algorithms. In subsequent discussion, both wideband and narrowband processing algorithms shall be discussed.

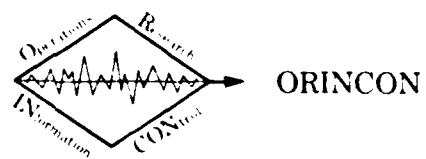
The basic function of the surveillance system is to detect a signal, whether it is narrowband or wideband. Because the signal-to-noise ratio (i.e., SNR) can be expected to be small, the detection



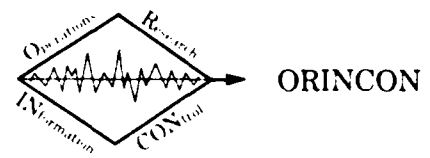
problem is difficult. A second important function of the system is to determine the direction from which the detected signal emanates. The detection and direction-finding requirements imply that an array of sensors should be deployed. Because of the time-varying character of the noise, adaptive array processing methods should be employed to achieve the system objectives. There may be several sources of coherent energy during any detection interval. Therefore, the directional noise cancelling capabilities of an adaptive array must be employed and should be particularly useful. Further, the data from an array can be used to estimate the average velocity of a detected signal as it passes the array location. The velocity estimates can be used, for example, as one feature for establishing the type of wave. The surveillance system, also, should provide information regarding the location of the source of a detected signal. This requirement implies the utilization of multiple arrays. By processing the outputs from more than one array, localization and tracking information can be deduced.

Mathematical models that are useful for developing signal processing algorithms are introduced in Part II. Basic models and the general problems are defined in Section II.1. Some fundamental aspects of array processing are discussed in Section II.2. In particular, the array pattern is defined and discussed as it provides a basic tool for evaluating the performance of a particular array configuration. The array processing problem is described in Section II.3 and the concept of array directivity is introduced. The conditions for arrays having maximal directivity are presented and discussed. Then, a statistical formulation of the optimal array processing problem is defined and a general solution is described in Section II.4. Additional aspects of array processing are introduced in this section also. Adaptive arrays are discussed; optimal detectors are introduced; and narrowband and broadband signals are considered.

The salient features of the seismic signal processing problem, discussed in Parts I and II, are summarized in Part III. General algorithms that are suitable for establishing the feasibility of the system



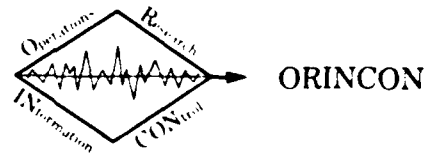
from experimental and/or simulated data are presented in Part III. One can proceed directly from this Introduction to Part III to avoid the lengthier discussions of the physical character of the problem and the major signal processing concerns. Emphasis in Part III is placed on the presentation of the general computations that must be accomplished to obtain the best performance of the signal processor. In addition, recommendations are provided for directions that should be taken for the detailed development of the signal processor.



PART I
BASIC PHYSICAL CONSIDERATIONS

ABSTRACT

Before defining algorithms that can be used in a seismic surveillance system for detection, classification, localization, and tracking of relevant objects and events, it is necessary to examine the character of the signals received by the sensors in order to assess the signal processing requirements. The fundamental properties concerning the propagation of seismic energy are reviewed in this section. The discussion shall focus upon those aspects that are most germane to the development of effective signal processing algorithms. More detailed expositions are provided, for example, in the books by Dobrin [1], Grant and West [2], Parasnis [3], Telford, et. al. [4], and Aki and Richards [5]. This presentation draws heavily from these references.



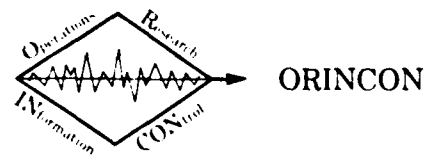
I.1 General Description of the Sensors

The seismic energy transmitted within the earth by a specific source is detected by a geophone. The output of this sensor generally can be regarded as being proportional to the velocity of the motion of the earth at the geophone in the direction of its sensitive axis.

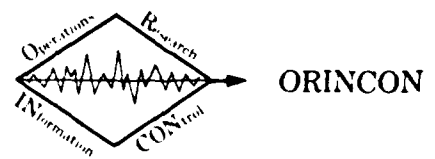
The natural frequency of a geophone is typically less than 10 Hz and may be as low as 1 or 2 Hz. The instruments exhibit a flat amplitude response and linear phase for frequencies between the natural frequency and, possibly, several hundred Hertz. The range of possible frequencies in each type of seismic wave is discussed below. It shall be assumed that the geophones are sensitive to the range of potential frequencies that may be encountered.

Motions in both horizontal and vertical directions are possible and can provide useful information. Consequently, three geophones can be mounted together to form a three-axis geophone. Typically, the sensitive axes are aligned to be orthogonal to one another. Then, the three-axis geophone is placed on or near the surface of the earth with one geophone oriented vertically and with the two remaining geophones located in the horizontal plane. In the subsequent discussion, reference will be made to particle motions in the horizontal (i.e., X and Y directions) and vertical (i.e., Z direction) directions in implicit reference to this assumed orientation.

The signal received by a geophone generally can be expected to be small relative to the noise. To enhance the signal, arrays of geophones are formed whose outputs, when combined in an appropriate manner, produce a greater SNR in the composite signal than in the elementary signal obtained from a single sensor. The array configuration can be defined in a variety of ways. Questions of this nature are an integral part of the design of the signal processor and will be considered later in the discussion.



It is also natural to consider more than one array. In other words, it is desirable to consider the placement of arrays at widely separated locations. The outputs of each array can provide a significantly different view of a source to assist not only with detection but with localization and tracking. Because of the existence of arrays of sensors, the spatial characteristics of the propagation of seismic energy must be considered. However, the discussion of the signal processing problem presented in this report is restricted to a single array. Multi-array processing, while an important topic, is beyond the scope of the current effort.



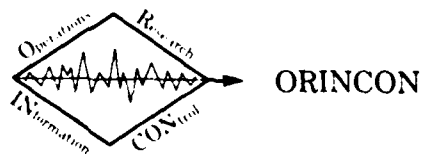
1.2 Basic Modeling Assumptions

The mathematical analysis of the propagation of seismic energy begins by considering an idealized model of the earth that can be used to obtain fundamental insights. Then, the effect of deviations from the ideal can be considered to obtain an understanding of the propagation for more realistic models. Fundamental to these analyses is the assumption that the earth is an elastic medium. Consequently, one is concerned primarily with the nature of elastic-wave propagation. This assumption imposes a linear character upon the channel characterization that is important from the point-of-view of the signal processor.

The propagation of seismic energy occurs through particle deformations that travel through the earth at velocities that are determined by the elastic properties and densities of material. The deformations are analyzed in terms of stress and strain (i.e., the forces that cause the deformations). The analysis leads to the development of the wave equation as the descriptor of the particle motion.

The elastic nature of the material provides the conclusion that there are two basic types of waves that must be considered, compressional waves and shear waves. Generally referred to as body waves, the propagation of these waves must be investigated to establish the manner in which the seismic energy is absorbed and attenuated by the material.

Wave propagation is studied by assuming an idealized earth composed of horizontal layers of materials with radically different elastic properties. The interface between layers is assumed to be described by a discontinuous change in the elastic properties. Within a layer, it is commonly assumed that the material is homogeneous and isotropic. With this model, the propagation paths for the body waves can be analyzed in terms of their reflection and refraction characteristics at the interface boundaries.



In addition to the compressional and shear waves, a Rayleigh wave travels along the free surface of the earth. As discussed below, the Rayleigh wave is, generally, the strongest wave generated by a compressional source. The layering of the earth can permit the existence of another surface wave, the Love wave. The Love wave is observed when a low-velocity layer overlays a higher-speed layer. Information regarding the surface or weathered layer can be obtained from the Love wave.

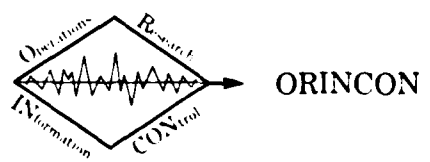
Deviations from the idealized model can complicate the analysis in a significant fashion. Imperfectly elastic, non-isotropic, or non-homogeneous materials must be considered. Layering generally will not be perfectly horizontal. In fact, the interface may not be represented as a discontinuous change in elastic properties of adjacent materials. Some of these aspects shall be discussed in Section I.4 as they complicate the models upon which the signal processor is based.

I.3 Basic Wave Characteristics

In the context of the idealized assumptions stated in Section I.1, characteristics of the basic types of waves shall be stated for future reference. In particular, the following characteristics shall be considered:

- a) Direction of particle motion: Each wave travels by deforming the materials in particular ways. The geophones detect the deformations along each of the sensitive axes of the instruments. Consequently, it is important to identify the direction of motion induced by a wave as a potential classification method.
- b) Speed of the wave front: Different waves travel with different velocities. It is useful to establish ordering relationships among the wave types.
- c) Dispersive waves: The speed of a wave can vary with frequency. As a result, the shape of the wave train changes as the distance of travel increases thereby adding a significant complication to the correlation of outputs from different arrays.
- d) Energy attenuation with range: The wave energy diminishes with distances of travel due to a variety of effects. For example, the earth acts as a low pass filter whose cutoff frequency diminishes with range. The manner and magnitude of the attenuation helps to define the required signal processing gain.

In this section, the four basic characteristics defined above shall be described for compressional, shear, Rayleigh, and Love waves. Emphasis is placed on the characteristics that assist in discriminating between wave types.



1.3.1 Compressional Waves

Compressional waves are also referred to as P-waves, longitudinal waves, or dilatational waves. Impulsive sources generate, primarily, compressional waves. Shear waves, as discussed below, are produced at interface boundaries.

- a) Direction of particle motion: Particle motion for a compressional wave is always along the direction of travel of the wave. It consists of alternating condensations and rarefactions of the material.
- b) Speed of wave front: Ideally, the wave propagates away from the source as an expanding sphere, at least through the initial layer. The velocity of the wavefront can be expressed as

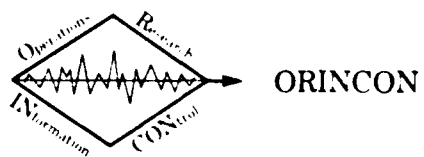
$$v_p = \sqrt{\frac{k + 4\mu/3}{\rho}}$$

where k = bulk modulus

μ = shear modulus

ρ = density

The speed of a compressional wave varies, typically, from 300 to 800 m/sec. in sand to 4,000 to 7,000 m/sec in granite. One sees that a variation in speed of at least one order of magnitude is possible depending upon the type of material. The speed also depends upon the depth of the material and upon its "lithology." Consequently, the speed can be very different within materials that are classified as the same. It is important to note that this variation implies that it is very unlikely that propagation speed can be regarded as known for a deployed surveillance system unless circumstances permit a thorough calibration.



- c) Dispersive: Compressional waves are generally regarded as nondispersive. Thus, the speed of the wave front does not change significantly with frequency.
- d) Energy attenuation with range: As a spherical wave propagates from a source, the energy of the wave is distributed over the area of the sphere. As the radius increases, the energy/unit area must diminish as the square of the radius. Thus, the amplitude of the wave (i.e., the square-root of the energy) is inversely proportional to its distance from the source.

In addition to the attenuation of the wave energy due to geometrical spreading, losses also result from absorption of energy by the transmission medium. Absorption losses are described approximately by an exponential function

$$A = A_0 \exp(-\alpha r)$$

where A represents the amplitude for a given wavelength, α is the absorption coefficient, and r is the distance to the source. The absorption coefficient is roughly proportional to frequency. Thus, the absorption is greater for higher frequencies and results in a low-pass characteristic for the earth. A reasonable value might be 0.25 dB/wavelength.

To indicate the relative effects of spreading and absorption, Telford, et al. [4] provide a table (p. 242) that indicates energy losses as a function of distance and frequency for a specific example. This table is reproduced on the following page (Table I.3-1).

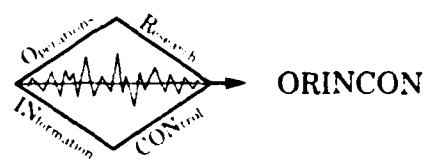
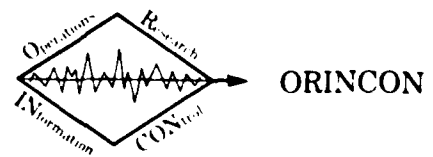


Table 1.3-1.
 (Telford, et al. [4])
 $\alpha = 0.25$ dB/wavelength, $V = 2000$ m/sec.

		Distance from Shotpoint			
		1200 m	2200 m	4200 m	8200 m
	Frequency (Hertz)				
Absorption	1	0.55 dB			
	3	1.60	3.3	6.6	13
	10	5.50	11	22	44
	30	16	33	66	130
	100	55	110	220	440
	All	16	21	26	32
Spreading					



The attenuation with frequency due to absorption is severe. Also, the absorption loss as distance increases dominates the spreading loss except at very low frequencies. It appears that the energy from a compressional wave will be extremely small at the ranges anticipated for the seismic surveillance system (i.e., 10 to 20 km).

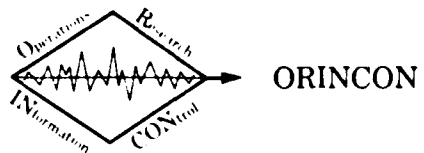
There are also energy losses caused by partitioning of the wave front at interface boundaries. The description of the partitioning depends upon the elastic properties of the adjoining materials and upon the angle of incidence of the wave upon the interface. As indicated in Reference [4] (e.g., Section 4.2.2m), the description of this energy loss is very complicated but substantial losses can result.

1.3.2 Shear Waves

The second major type of body wave is the shear wave. These waves are also referred to as transverse, rotational, or S-waves.

- a) Direction of particle motion: The particle motions for a shear wave are orthogonal to the direction of travel of the wave. Whereas particle motion for a compressional wave is one-dimensional, there are two degrees of freedom for the particle motions of a shear wave. The motion can be polarized to be contained in a plane. The motions can be resolved into components parallel to and perpendicular to the surface of the earth. The components are referred to as SH and SV waves.
- b) Speed of the wave front: The velocity of a shear wave front is given by

$$v_s = \sqrt{\frac{G}{\rho}} .$$



Comparing this speed with the speed of a compressional wavefront as given earlier, it follows that

$$\frac{V_P}{V_S} = \sqrt{\frac{k}{\rho} + \frac{4}{3}} .$$

Clearly, a shear wave travels more slowly than a compressional wave. For most rock formations, the ratio is bounded as

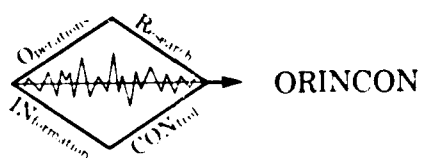
$$1.5 < V_P/V_S < 2.0 .$$

- c) Dispersive: Shear waves are generally regarded as non-dispersive.
- d) Energy attenuation with range: The remarks given for compressional waves apply as well for shear waves.

I.3.3 Rayleigh Waves

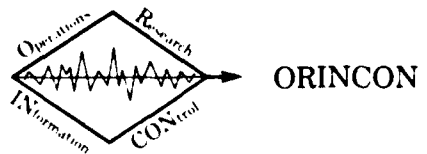
Rayleigh waves travel along the free surface of the earth. In many situations the Rayleigh wave is the strongest wave generated by the source. Consequently, this wave should play an important role for seismic surveillance.

- a) Direction of particle motion: Particle motion of a Rayleigh wave is always in the vertical direction. Furthermore, the motion is elliptical and retrograde (i.e., counterclockwise) with respect to the direction of motion. Thus a Rayleigh wave will be sensed by both a horizontal and a vertical geophone. Because of the retrograde motion, a phase difference of 90° will exist between the two geophones. The sign of the difference depends upon the orientation of the horizontal geophone relative to the direction of travel of the wave.



- b) Speed of wave front: The speed of a Rayleigh wave is less than for either type of body wave. It is approximately equal to nine-tenths of the speed of a shear wave.
- c) Dispersion: Generally, the Rayleigh-wave velocity varies with frequency (i.e., it is dispersive). For wavelengths that are small compared with the thickness of the surface layer, the speed is approximately nine-tenths of the shear velocity in the surface layer. For long wavelengths, the speed is nine-tenths of the shear velocity in the substratum. The velocity for medium wavelengths is intermediate to the velocities at short and long wavelengths.
- d) Energy attenuation with range: The Rayleigh wave is the strongest wave generated by a compressional source and its energy attenuates much less rapidly than for compressional or shear waves. Because of its essentially two-dimensional nature, the geometrical attenuation of the amplitude is proportional to the square-root of the distance, $r^{-\frac{1}{2}}$, rather than r as for P- and S-waves. The Rayleigh wave experiences absorption losses, particularly at higher frequencies. Generally, the Rayleigh wave is observed at a distance from the source as a low frequency motion (e.g., less than 10 Hz). The time duration of this dispersive wave is long relative to compressional and shear waves. Note, also, that a Rayleigh wave can suffer no partitioning losses since it is a surface wave.

The Rayleigh wave may be the principal energy source for a seismic surveillance system. However, it is the most slowly moving wave so its arrival should be pre-saged by earlier arrivals of other types of waves. The characteristic motion of the Rayleigh wave should permit

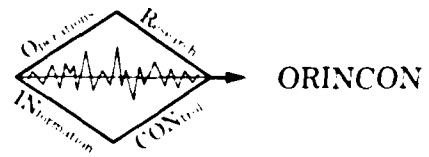


its classification by the signal processor. The dispersive nature of the wave may hinder the use of correlation techniques for measurements obtained from different arrays.

1.3.4 Love Waves

The layering of the earth can induce a wave-guide effect when a low-speed material overlays a higher-speed substratum. A surface wave called a Love wave is generated.

- a) Direction of particle motion: Particle motion for a Love wave is contained entirely in the horizontal plane and is orthogonal to the direction of travel of the wave. Thus, a vertical geophone will not sense the passage of a Love wave.
- b) Speed of wave front: The speed of a Love wave is intermediate between the shear wave velocity at the surface and the shear wave velocity in the substrata. Generally, the Love wave will have a greater velocity than a Rayleigh wave so the Love wave will arrive at a geophone before the Rayleigh wave. However, the energy of the Love wave is usually substantially less than for a Rayleigh wave.
- c) Dispersive: Love waves are dispersive with greater velocity at longer wavelengths.
- d) Energy attenuation with range: The Love wave can be regarded as an SH wave (i.e., a shear wave polarized to the horizontal plane) and suffers attenuation in the manner described in Section 1.3.2.



I.4 Propagation Paths

Seismic energy can be propagated from a source to a sensor along a number of different paths. Three basic propagation paths (i.e., direct, reflections, and refractions) are considered in this section. Single and multiple reflections are discussed as are the refractions that generate head waves.

I.4.1 Direct Waves

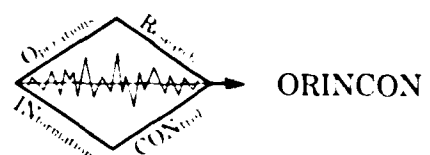
A primary propagation path for seismic energy is the direct wave. Direct waves are transmitted in the surface layer of the earth and do not interact with any interface boundaries between layers. The Rayleigh and Love waves described in Section I.3 exist only as direct waves. However, compressional and shear waves can also travel directly from the source to the sensor. Among the four direct waves, the compressional wave will arrive at the sensor first with the shear and Love waves arriving next. The Rayleigh wave should be the last to arrive. Since it has the greatest energy, it generally is the easiest to detect.

The direct compressional and the Love waves are sensed only by the horizontal geophones whereas the direct shear, if it exists, and the Rayleigh waves can also be detected by the vertical geophone. With two horizontal geophones, the direction of arrival of a wave can be determined, conceptually at least. For example, a compressional wave detected on one horizontal geophone but not the other obviously defines the direction of arrival. Arrival at a 45° angle is heralded by the simultaneous arrival of the same signal at each geophone.

For a direct wave traveling with velocity V , the travel time t_D from source to sensor is

$$t_D = \frac{x}{V}$$

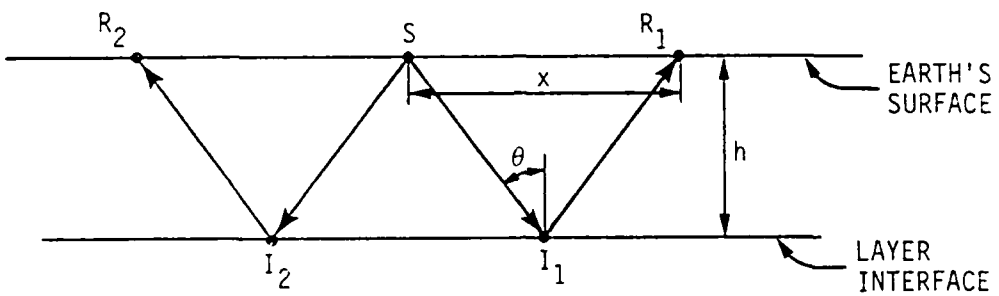
where x represents the distance from the source to the sensor.



The time-of-arrival of the same wave at different sensors is seen to be a linear function of the distance x . As is discussed below in Section 1.4.2, this linear characteristic across array elements can provide a mechanism for discriminating between direct and indirect waves.

1.4.2 Reflected Waves

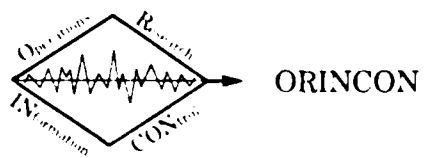
Consider the following diagram and suppose that the seismic source is located at S and that geophones are located at R_1 and R_2 .



The arrows define a ray path for the wave which encounters a layer interface boundary at I_1 and I_2 . Some of the energy is reflected back into the surface layer. Although not indicated, some of the energy is refracted into the second layer. The energy partitioning depends upon the angle of incidence and upon the properties of the layers.

The angle of reflection for the wave equals the angle of incidence. If the wave velocity is V , the layer thickness is h , and the source-sensor separation distance is x , the travel time t_R must satisfy

$$t_R = \frac{\sqrt{x^2 + (2h)^2}}{V}$$



or

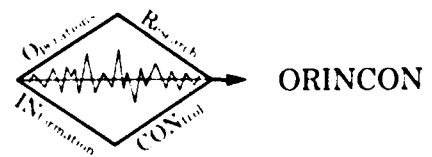
$$\frac{v^2 t_R^2}{4h^2} - \frac{x^2}{4h^2} = 1 .$$

Thus, the travel time is described by a hyperbola and the difference in arrival times at different sensors is obtained from this quadratic relationship.

The arrival times across an array for reflected waves exhibit a markedly different characteristic than do the arrivals of direct waves. Furthermore, a direct wave of a particular type must arrive at the sensor sooner than for this reflected (i.e., they are equal only for $h=0$). The partitioning of energy at the interface boundary causes the reflected wave to contain less energy than the direct wave. This reduction is accentuated by the fact that the reflected wave travels a greater distance in the same layer than the direct wave.

Because of the reflection angle, a compressional wave generally will be detected on the vertical as well as the horizontal geophones. In addition, a compressional wave is partitioned at a boundary into both reflected compressional and shear waves. The reflected shear wave will arrive later than the compressional wave and, if it has sufficient energy, be detected by both horizontal and vertical geophones.

The reflection phenomena can be repeated at the boundaries of lower layers with the refracted waves that enter each subsequent layer. Thus, the signals arriving at the sensor may be the result of one or several reflections. The difference in travel times may cause an overlapping of two signals leading to the apparent lengthening of a single signal or may lead to the appearance of two disjoint signals. The time separation of different reflections of the same signal depends upon the width and character of the layers.



These characteristics generally must be unknown for a seismic surveillance system. The energy contained in multiply reflected waves often will be considerably less than for direct or singly reflected waves because of the partitioning and travel distances.

1.4.3 Refracted Waves

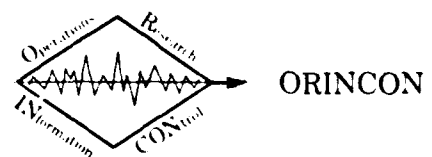
Seismic energy can be either reflected or refracted at the boundary between layers having different elastic properties. Letting V_1 and V_2 represent the wave velocity in two adjacent layers, the angle of refraction θ_2 is determined using Snell's law. In particular, it is known that

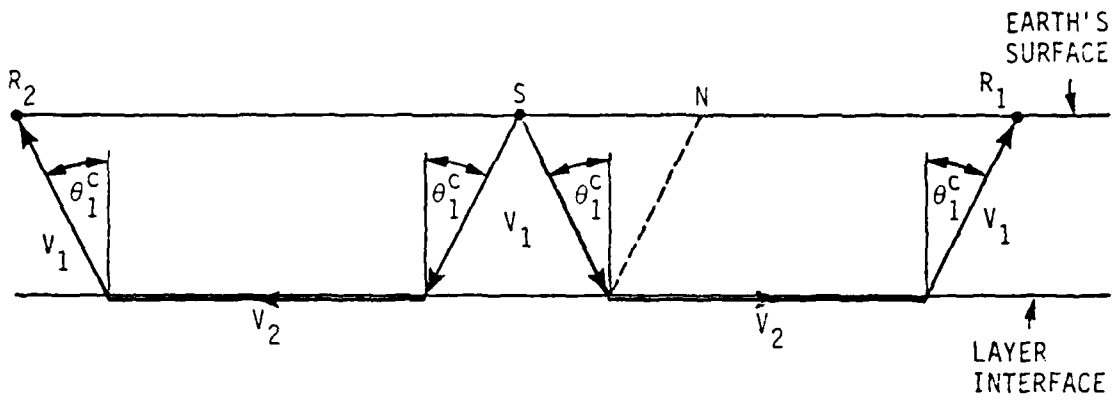
$$\frac{\sin \theta_1}{V_1} = \frac{\sin \theta_2}{V_2} .$$

When the underlying layer permits a greater wave velocity (i.e., $V_2 > V_1$), the refracted wave can travel along the interface at the velocity V_2 . This occurs when the angle of incidence satisfies

$$\sin \theta_1^c = \frac{V_1}{V_2}$$

thereby causing $\sin \theta_2 = 1$ (or $\theta_2 = 90^\circ$). The refracted wave that is generated at this critical angle θ_1^c is referred to as a head wave. From Huygen's principle, the head wave causes energy to be propagated in the overlying layer and to return to the surface. This situation is depicted in the following figure.





The head wave is significant since the higher velocity V_2 can permit this energy to arrive at the geophone earlier than any direct wave. From the diagram, it should be apparent that head waves are not possible in the interval SN. For seismic surveillance, the separation distance x between the source and the sensor should be sufficiently large that $SR_1 > SN$ and head waves may be a significant carrier of energy for the geophones.

Travel time t_H for a head wave traveling a horizontal distance x can be expressed as

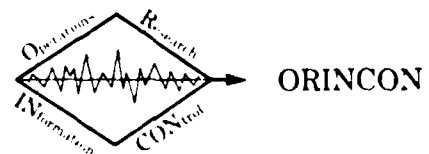
$$t_H = \frac{x}{V_2} + t_1$$

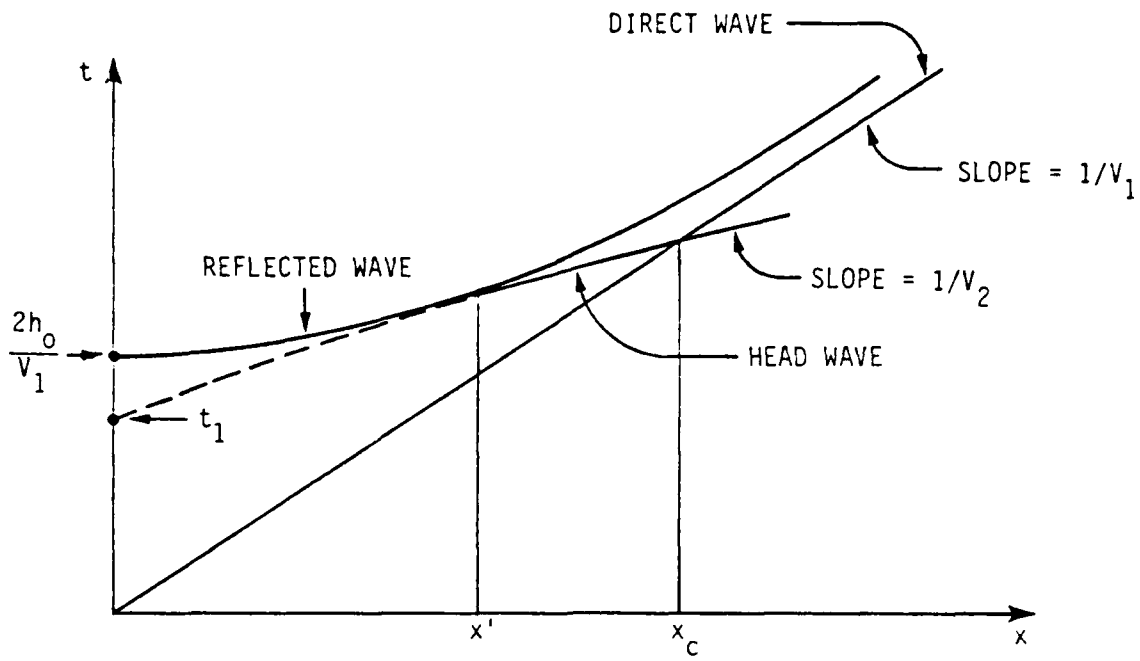
where

$$t_1 = 2h \cos \theta_1^c / V_1 .$$

The parameter h represents the thickness of the layer and θ_1^c , V_1 , V_2 have been defined above. The travel time is seen to be a linear function of the separation distance x with slope $1/V_2$ and intercept time t_1 .

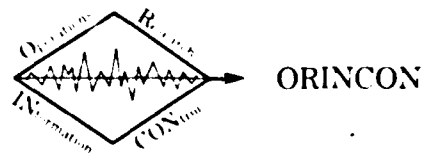
To illustrate the relation between arrival times for different propagation paths of the same wave, consider the following diagram.





For separation distances less than x' , no head waves are possible. Thus, the direct wave provides the initial energy received by the sensors at distances $x < x'$ and the signal is augmented at a later time by the arrival of the reflected energy. For sensors with separation distances between x' and x_c , the direct wave continues to be the first arrival with the head and reflected waves arriving subsequently. The head wave always precedes the reflected wave. For sensors beyond the crossover distance x_c , the head wave arrives first and is followed by the direct and the reflected waves. At the greater distances, the reflected wave assumes a linear characteristic (i.e., asymptotically) and must also arrive after the direct wave.

The discussion can be extended to consider the effects of multiple layers. At each interface, the incident wave is partitioned into reflections and refractions. Head waves are possible at every boundary at which a lower velocity layer overlays a higher velocity layer. The refracted waves generated at the first layer are partitioned at the next layer. Thus, the mechanism can repeat as long as energy remains or until the layering ceases.



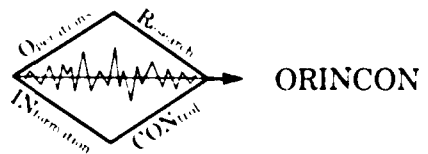
1.5 Error Sources

The conclusions described above are obtained through the analysis of an idealized model of the earth. Realistically, many deviations from the modeling assumptions are possible and their effects must be considered in any signal processing design. In this section, some major error sources are reviewed to provide an indication of their significance and of possible compensation mechanisms.

1.5.1 The Low Velocity Layer (LVL)

Generally, the surface layer of the earth exhibits propagation velocities that are comparable or less than the velocities in water (i.e., 250 m/sec to 1000 m/sec). Within this low velocity layer, the propagation of seismic energy is characterized by several troublesome properties. First, the velocity is highly variable in this layer and this variability can affect the travel times. Also, the width of the layer can change substantially between the source and the sensor (e.g., elevation changes). In addition, absorption of seismic energy can be quite high thereby greatly reducing the effective propagation range. The absorption can effectively limit the reflected energy to be restricted to nearly vertical paths. Since the layer below the LVL often has radically different elastic properties, the interface will act as a strong reflector. Then, the refracted energy is less than at other interfaces thereby reducing the energy in the head wave or in multiple reflections.

The energy source for seismic surveillance generally is located on the earth's surface (or flying above it). Thus, the effects of the LVL must be considered and often will be the primary physical factor limiting the effective range of the system. Whenever possible, it will be desirable to compensate or to correct for the influences of the LVL.



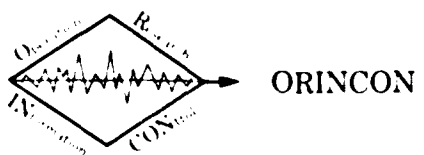
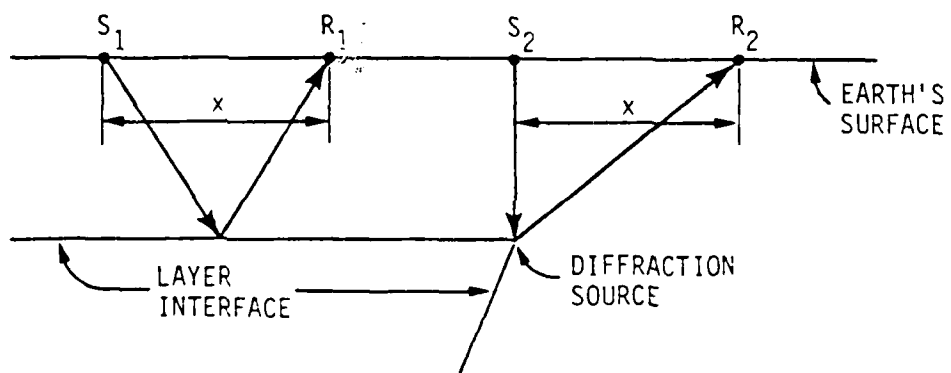
1.5.2 Dipping Layers

The assumptions that the layers of the earth are horizontal is an idealization often violated in the field. Travel time characteristics for reflections from a dipping subsurface are similar to but different from the result stated in Section 1.4.2. In particular, the travel time is still a hyperbolic (i.e., quadratic) function of the separation distance x , but the axis of symmetry is no longer given by the time axis. That is, the travel time is different for geophones located symmetrically about the source. This effect must be recognized if reflected or refracted waves are used in a localization scheme.

1.5.3 Diffractions

Whenever a wave encounters an irregularity whose radius of curvature is less than the wave length, the energy is diffracted according to Huygen's principle. Thus, energy is propagated in all directions from the irregularity. A diffracted wave will first reach the surface at a point directly above the irregularity. The travel times increase with the distance from this point in a manner that makes it indistinguishable from a reflection.

Consider the following diagram:



The travel time for the reflected wave, as indicated earlier, is

$$t_R = \frac{1}{V} (x^2 + 4h^2)^{\frac{1}{2}} \approx \frac{2h}{V} + \frac{x^2}{4Vh} .$$

For the diffracted wave with S_2 directly above the irregularity, the travel time is

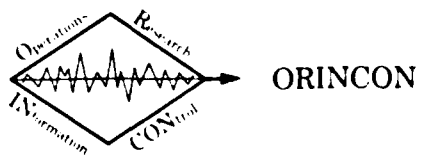
$$t_{\text{DIFF}} = \frac{1}{V} [h + (x^2 + h^2)^{\frac{1}{2}}] \approx \frac{2h}{V} + \frac{x^2}{2Vh} .$$

Thus, the diffracted wave appears the same as the reflected wave but the apparent depth of the reflector differs by a factor of two.

The LVL, dipping layers, and diffraction irregularities represent three major sources of potential errors for the signal processor but many others are possible. Certainly, inelasticities, nonhomogeneities, and/or anisotropies will introduce changes in the propagation characteristics that have been described. However, even the consideration of these three error sources serves to emphasize the difficulties inherent in detecting events and determining source locations from the highly complex signals that arrive at the sensors. Fundamentally, the signal processor is concerned with detecting events characterized by low signal-to-noise ratios and with distinguishing between direct waves, reflected waves, refracted waves, diffracted waves, and multiples.

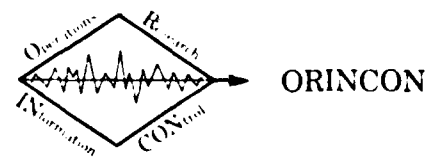
I.5.4 Noise Sources

The noise background against which a source signal must be detected is itself complex. One can regard the noise as being either incoherent or coherent. Coherent noise is defined to represent energy that has characteristics that will be recognizably



similar in several elements of the sensor array. In many instances, this energy may be generated by a specific source much as the energy for the signal source. But in focusing upon a particular source, energy from other potential sources becomes interference and is a nuisance that must be eliminated. Noise which appears dissimilar in different sensors is defined as incoherent and conforms with the more standard description of random noise.

The effects of incoherent noise in different sensors can be reduced simply by adding sensor outputs. The cancellation effect is proportional to the square-root of the number N of sensors, \sqrt{N} . The attenuation of coherent noise can be accomplished by methods which depend either upon knowledge of its characteristics (i.e., filtering) or upon the directivity of the source (i.e., beam forming). Suppression of both coherent and incoherent noise is a basic objective of the signal processing and shall be discussed later as the signal processing algorithms are defined.



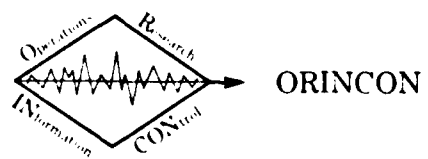
1.6 Some Basic Modeling Considerations

Based on the preceding discussion, it is useful to attempt to formulate modeling concepts that can serve to provide direction to the development of appropriate signal processing algorithms. These general, qualitative remarks are appropriate before introducing any detailed mathematical considerations.

Suppose the source is basically impulsive (e.g., a shell blast or an artillery recoil). Then, the signal introduced into the earth should have a short duration with the largest amplitudes appearing at the start of the signal and decaying rapidly to zero thereafter. Thus, the frequency content of the input signal is rich, and a relatively broadband signal should be expected. From the preceding discussion, it is unreasonable to expect that the signal received at the sensor will have the same shape or character as the original signal. The signal distortion results for a variety of reasons.

The apparent time duration of a received signal can be relatively long because of the variety of propagation modes and paths that are possible. The concatenation of direct, reflected, and refracted waves of different types induces a total signal duration greatly in excess of the primary signal. Further, the time duration of the low-frequency Rayleigh wave is itself lengthy. Thus, the observed signal can appear as a persistent signal that is not consistent with the assumed impulsive character of the source.

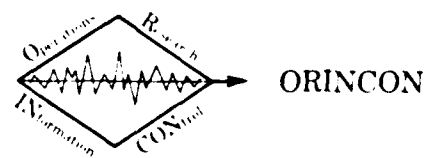
For the remainder of the discussion, the following notation is introduced. Consider the signal received by a single geophone and denote this signal as $s_{ij}(t)$. The subscript i ($i=1,2,3$) is used to denote the specific component of the three-dimensional geophone. For convention, we shall assume that $i=3$ denotes the vertical geophone. The subscript j ($j=1,2,\dots,N$) denotes the j^{th} element in an array composed of N three-dimensional geophones. The symbol $s_j(t)$ shall be used to denote the three-dimensional signal at the j^{th} element.



The primary signal will be regarded as the signal arriving at the geophone as a result of a single propagation mode and associated with a single propagation path. For example, the primary signal for a Rayleigh wave could be denoted as $s_{ij}^R(t)$ and is characterized by its arrival time t_{ij}^R at the j^{th} array element and the i^{th} geophone. Every primary signal is assumed to be identically zero prior to arrival time.

The signal that is observed through the output of a specific sensor reflects the arrival of several primary signals. Because of the basic assumptions regarding the elasticity of the earth, the primary signals can be assumed to combine linearly (i.e., they are additive). Moreover, a primary signal $s_{ij}(t)$ is obtained as a linear convolution of the original source signal with the impulse response (i.e., a Green's function) of the earth. The impulse response will depend upon the propagation path, propagation mode, and distance for the reasons given above. For example, the energy in the signal is attenuated due to spreading, absorption, and partitioning effects. Secondly, the earth has a low pass filtering effect. Consequently, the broadband nature of the original signal is reduced with the filtering effect increasing as the source/sensor separation increases. Even with the reduction in the frequency bandwidth of the signal, the effective time duration of the primary signal remains relatively brief (i.e., a few seconds). Finally, the dispersive nature of some waves can cause fundamental changes in the character of the wave form.

The signal received along each axis of a three-dimensional geophone represents the projection of the direction of the particle motion upon the geophone axis. The signal $s_j(t)$ can be defined in terms of the direction of arrival of the signal. One is concerned, principally, with the direction of arrival as defined in the horizontal plane (i.e., the x-y plane as defined by the horizontal geophones). It is this angle that defines the direction from the geophone to the source and provides the basic mechanism for localization. The

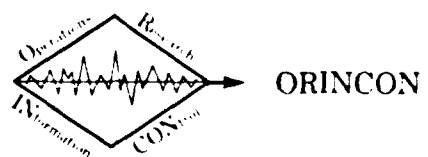


deflection of the arrival direction below the horizontal (i.e., the signal measured by the vertical geophone) provides information that is useful for classifying the type of wave that is received at a particular time t_{ij} .

To conclude the discussion, it is useful to consider the basic information to be produced by the signal processor. In essence, the processing must provide the type of information that is typically displayed in a space-time plot. For example, the analysis of seismic records is aided by the simultaneous plotting of the outputs of several geophones as a function of elapsed time and distance from the sensor to the source. The amplitude of the output can be reflected by the darkness of the plot at each point. The following figure is taken from Grant and West [2] and provides a graphical illustration of some of the ideas that have been introduced. Note that the origin of the plot represents the location of an impulsive source (i.e., a shot).

The linear characteristic of the direct wave and other more slowly moving surface waves is seen clearly. The appearance of a head wave with its linear characteristic and crossover point can be seen. Also, the hyperbolic characteristic of a reflected wave is shown in this figure. In addition, a continuously refracted wave is observed.

Consideration of this figure should serve to re-emphasize the complexity of the seismic signals that are obtained from an array of geophones. The arrival times provide the information of basic interest for the analysis although the shortness of the signal appears to permit the separation of different propagation modes and paths. The availability of spatial measurements (i.e., the existence of arrays) obviously is mandatory for any localization. We note also that the data presented in this figure have been subjected to considerable processing and do not represent the "raw" data obtained from



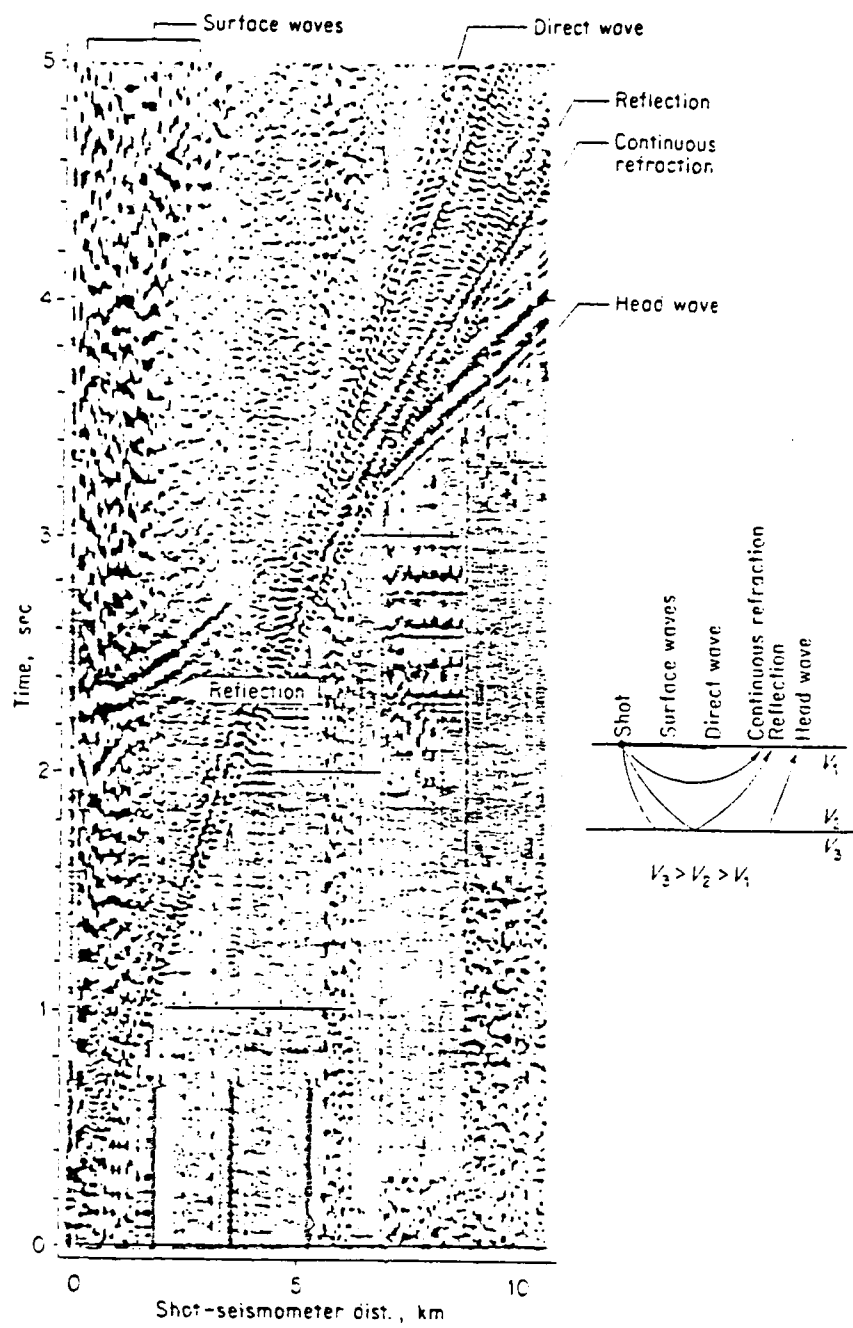
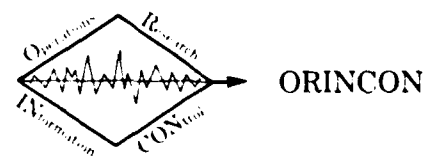


Figure I.6-1. (p. 112) from Grant and West [2].

the sensors. In concept, the signal processor must be capable of producing the type of information implicit in this diagram. Clearly, the existence of a source signal is apparent and the location of the source has been identified.

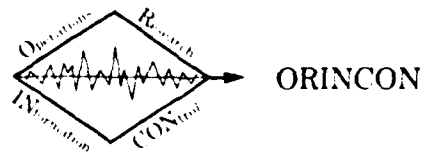


PART II

GENERAL SIGNAL PROCESSING CONSIDERATIONS

ABSTRACT

The definition of signal processing algorithms must be motivated through appropriate assumptions regarding the signal and the output noise processes. Fundamental properties of the signals have been discussed in Part I. As indicated there, the signals must be expected to have an unknown form that results from the many and complicated propagation paths of the energy produced by the target source. Thus, the signal processing algorithms must be developed using minimal assumptions regarding the character of the signals and of the output noise. Reasonable modeling assumptions are introduced in this section. These assumptions are used to develop detection and estimation algorithms that are compatible and consistent with the environment in which a seismic surveillance system must operate. In developing these algorithms, attention is directed to many concerns that are fundamentally important to achieve the most rapidly convergent adaptive array processing algorithms.



II.1 Mathematical Models and Problem Definitions

II.1.1 The General Problem

To provide a framework for the discussion, assume that a rectangular coordinate system is defined with prescribed origin and axes x-east, y-north, and z-vertical to form a right-handed system. The location of each sensor is defined in terms of this system. That is, the position \underline{r}_i of the i^{th} sensor in the array ($i = 1, 2, \dots, N$) is given as

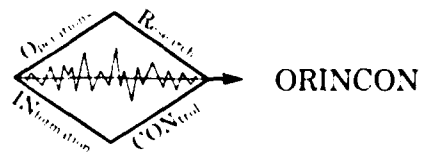
$$\underline{r}_i = x_i \underline{i}_x + y_i \underline{i}_y + z_i \underline{i}_z. \quad (2.1)$$

Throughout, it is assumed that there are N geophones, possibly 3-axis, located essentially on the surface of the earth. The origin is defined to be located on the earth's surface with the consequence that $z_i \equiv 0$ for all i . The components x_i , y_i are defined by a distance r_i and an azimuth angle θ_i , as discussed below.

For the array dimensions and propagation distances that are reasonable for the seismic surveillance system, the signals measured at each sensor can be assumed to be generated by a plane wave propagating with speed c across the array in a direction $\underline{\beta}$, where

$$\underline{\beta} = \beta_x \underline{i}_x + \beta_y \underline{i}_y + \beta_z \underline{i}_z; \quad \beta_x^2 + \beta_y^2 + \beta_z^2 = 1. \quad (2.2)$$

The vector $\underline{\beta}$ represents the normal to the wavefront as it passes the array. The form of the signal received by the array elements cannot be assumed to be known. In comparable elements (e.g., the vertical seismometers), it is reasonable to assume that the basic character of the signal is similar, differences being caused primarily by propagation delays caused by geometric effects. The form of the signal may be different along the sensitive axes of a 3-axis geophone for the reasons discussed in Part I of this report and reconsidered below.

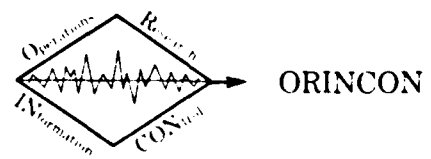


To simplify the notation, consider an array composed entirely of vertical seismometers. Because of the common orientation of the sensors, the signal, denoted by $s(t)$, that would be received at the origin of the coordinate system is also received at each seismometer at a suitably delayed time. Specifically, the received signal at the i^{th} sensor located at \underline{r}_i can be represented as

$$s_i(t) = s \left(t - \frac{\beta^T \underline{r}_i}{c} \right), \quad i = 1, 2, \dots, N. \quad (2.3)$$

By referring to (2.3), essential aspects of the problem can be identified. From the received signal one wants to determine the direction β and the wave speed c . Both are unknown and only the sensor location \underline{r}_i is known. Note that in a practical system there generally will be uncertainty regarding the exact location of the sensor.

The sensor output will differ from the signal $s_i(t)$ because of noise effects $n_i(t)$. The noise can be regarded as the composite of two disparate processes. There can be coherent or directional noise $n_i^C(t)$ that emanates from some point source of seismic energy. Because of its directional character, it is similar to the signal itself and can be regarded as being generated by a plane wave having some speed and direction. Secondly, there will be incoherent (i.e., omnidirectional) noise $n_i^R(t)$ that exists due to ambient conditions or sensor electronics. This noise component generally will be described as a stationary random process with zero mean. The sensor noise shall be assumed to be statistically independent between sensors of the array unlike the coherent noise. The mathematical assumptions imposed on the signal and the coherent and incoherent noise will be discussed in the subsequent sections.



To summarize, the i^{th} sensor output shall be denoted as $z_i(t)$ and it is assumed to be the sum of the signal and noise.

$$z_i(t) = s_i(t) + n_i(t) \quad (2.4)$$

where

$$n_i(t) = n_i^C(t) + n_i^R(t). \quad (2.5)$$

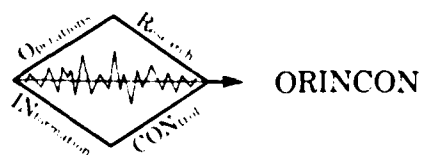
Implicitly, any term s_i , n_i^C , n_i^R can be absent in the output signal. This realization provides the basis for defining the problems that must be addressed in developing the signal processor.

Detection Problem

The signal $s_i(t)$ might not be present in the sensor output $z_i(t)$ during any time interval $T_0 < t < T_1$. When the signal is impulse-like (broadband), this will generally be the case. Thus, a time interval $(T_1 - T_0)$ must be considered in formulating the broadband detection problem.

Estimation Problem

The signal is characterized by a direction β and a speed c that is assumed to be common to the N sensor outputs when the signal is present. By estimating β , the direction of the source is established within the accuracy of the estimate. The estimate of the wave speed c provides a basis for identifying the type of wave that has passed the array. Further, an estimate of the signal itself or of its spectral characteristics provides some indication of the nature of the source.

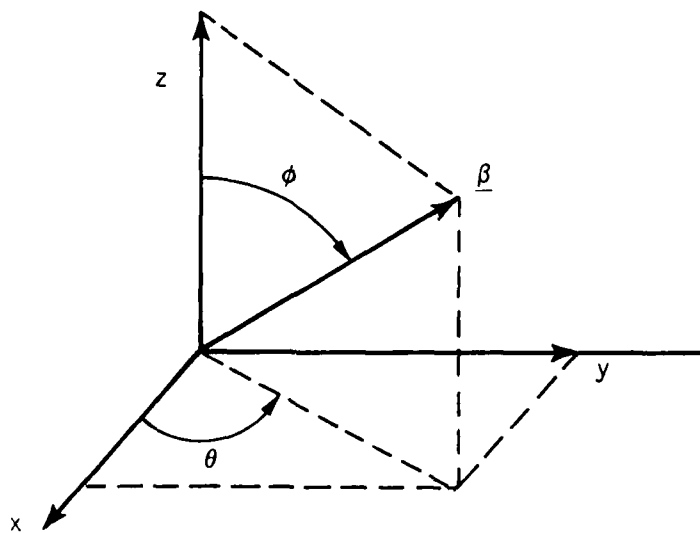


Signal Modeling Problem

For the mathematical analysis of the detection and estimation problems, mathematical models for the signal and coherent noise signals must be defined. But it is unreasonable to define very precise models for the signal because of the complicated nature of the propagation medium. Consequently, it is desirable to impose the least rigid assumptions possible about the signal model. Initially, we shall assume only that s_i and n_i^c have Fourier transforms and that n_i^R is a stationary random process with mean zero and correlation function $R_n(\tau)$. Other structural assumptions are introduced below in establishing some specific results.

II.1.2 Signals Generated by Seismic Waves

Consider the relation between the signals received at a sensor and the physical wave front that passes the sensor. Suppose that we consider a three-axis seismometer with the seismometers mounted orthogonally with a vertical seismometer oriented along the z-axis and two horizontal seismometers aligned with the x and the y-axes of the rectangular coordinate system defined earlier. The geometry is depicted below.



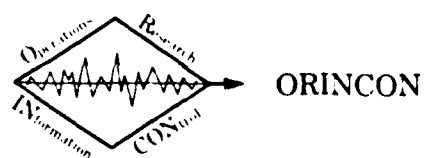
The vector $\underline{\beta}$ denotes the unit vector (i.e., $\underline{\beta}^T \underline{\beta} = 1$) defining the normal to the incoming wave front. The angle ϕ defines the cone angle measured from the z-axis. The angle ϕ is limited to the range 0° to 90° since waves approach the sensor through the earth. A surface wave occurs for $\phi = 90^\circ$ and a completely vertical wave occurs for $\phi = 0^\circ$. The azimuth angle θ is measured as positive counter clockwise from the x-axis and $0^\circ \leq \theta \leq 360^\circ$.

For this discussion, suppose that the sensors are aligned with the x, y, and z axes, respectively. Any other orientation could be considered but it only complicates the notation. Each sensor is omni-directional relative to particle motions that project onto the direction of the sensitive axis. For example, particle motions can be sensed by the vertical seismometer regardless of the azimuth angle θ as long as there is some vertical particle motion induced by the passage of the wave front.

Let us now consider the signals induced by the passage of P-waves, S-waves, Rayleigh waves, and Love waves, respectively.

P-Waves

A compressional wave induces particle motions along the direction of travel of the wave front. Suppose that a direct P-wave travels horizontally between the source and the sensor along the x-axis. Then, the passage of the wave front is sensed only by the x-seismometer and not by either the y-seismometer or by the vertical seismometer. Let the particle motion be denoted by the signal $s(t)$. In the absence of noise, the output of the seismometer triad would be the vector signal $\underline{s}^T(t) = (s(t), 0, 0)$. For an arbitrary P-wave, the direction of travel induces output signals that represent the projection of $\underline{\beta}$ onto the coordinate axes. In terms of ϕ and ψ , the noise-free output signal is given by



$$\underline{s}_P(t) = s_P(t) \begin{pmatrix} \cos \theta & \sin \phi \\ \sin \theta & \sin \phi \\ \cos \phi \end{pmatrix}$$

$$= s_P(t) \underline{\beta}. \quad (2.6-P)$$

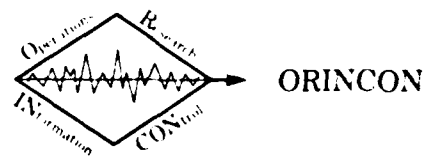
From (2.6-P) it is apparent that the outputs of a three-axis seismometer can be regarded as providing a direct measurement of the wave direction $\underline{\beta}$. There actually will be an ambiguity in the azimuth angle of 180° . If the system is composed only of vertical seismometers, then the output is $s(t) \cos \phi$. Direct P-waves (i.e., $\phi = 90^\circ$) are not sensed by the vertical seismometer.

S-Waves

The particle motions for a shear wave are orthogonal to the direction of travel of the wave. Whereas particle motions for a compressional wave correspond with the direction of travel, there are two degrees of freedom for the motions induced by a shear wave. These motions can be polarized to be contained in a plane. Then, the motions can be resolved into motions parallel to and perpendicular to the surface of the earth (i.e., the x-y plane).

In general, the motions induced by the passage of a shear wave can be regarded as more complicated than the P-wave motions. Often, the motions can be assumed to be polarized to the vertical plane (or to the horizontal plane). Then, the direction of the particle motions can be characterized by the unit vector $\underline{\gamma}$ where the noise-free output is

$$\underline{s}_S(t) = s_S(t) \underline{\gamma} \quad (2.6-S)$$



where $\underline{\gamma}$ is orthogonal to $\underline{\beta}$

$$\underline{\gamma}^T \underline{\beta} = 0.$$

In addition, the assumption that the waves are polarized to the vertical plane ensures that the normal to the plane defined by $\underline{\beta}$ and $\underline{\gamma}$ is orthogonal to the z-axis. Using vector cross-product notation, we have the condition that

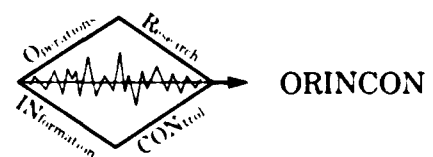
$$(\underline{\gamma} \times \underline{\beta})^T \underline{l}_z = 0$$

where \underline{l}_z is the unit vector defining the z-axis.

The two orthogonality conditions imply that θ and ϕ can be determined from $\underline{\gamma}$ except for a 180° ambiguity in θ . Consequently, the outputs of the seismometers provide a measurement of the wave direction $\underline{\beta}$. Note that a vertical seismometer will be sensitive to the passage of any shear wave other than a vertical wave. The existence of a vertical shear wave of interest for a seismic surveillance system is unlikely. Thus, an array of vertical seismometers is sufficient if the major source of energy is a shear wave. As indicated above, this type of an array is insensitive to direct P-waves. In many instances, the latter is more likely to contain sufficient energy to be detected than a shear wave.

Rayleigh Waves

Particle motion of a Rayleigh wave is always contained in the vertical plane. Furthermore, the motion is elliptical and retrograde (i.e., counterclockwise) with respect to the direction of motion of the wave. Thus, a Rayleigh wave will always be sensed by the horizontal and by the vertical geophones. Because of the retrograde motion, a phase difference of 90° will exist between the horizontal and the vertical geophones. The sign of the phase difference determines the direction of travel of the wave.



Because of the two dimensional nature of the Rayleigh wave, detection of a Rayleigh wave provides a direct measurement of the direction of the source. The existence of a Rayleigh wave can be established by observing a 90° phase difference in the outputs of the horizontal and vertical geophones. The direction of the source is determined from the sign of the phase difference.

Love Waves

Particle motion for a Love wave is contained entirely in the horizontal plane and, being a shear wave, is orthogonal to the direction of wave motion. Thus, a vertical geophone will not sense the passage of a Love wave. As discussed above for shear waves, detection of a Love wave implicitly provides a measurement of the direction of the wave front except for the ambiguity of 180° . The wave motion is characterized by the unit vector $\underline{\gamma}_L$ where

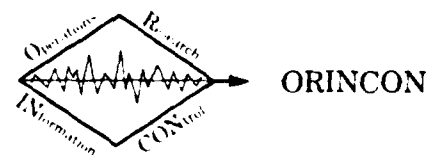
$$\underline{\gamma}_L^T \underline{\beta} = 0$$

and

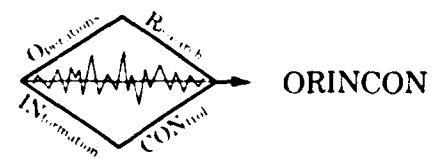
$$\underline{\gamma}_L^T \underline{1}_z = 0.$$

Clearly, $\phi = 90^\circ$ and $\theta = \theta_\gamma \pm 90^\circ$.

The noise-free outputs of a three-axis seismometer are described essentially by the time-varying scalar signal $s(t)$ as modulated by functions of the direction of the motion of the wave front. One could consider the array processing problem in the context of a vector output (i.e., the three-dimensional representation of the outputs of the three orthogonally oriented seismometers) from each array element. This formulation complicates the analysis and shall not be pursued here. Instead, we shall restrict attention to an array of scalar elements which, for the purpose of this discussion, are assumed to be vertical



seismometers. The discussion can be extended to 3-axis geophones without great difficulty by incorporating the considerations mentioned above. Potentially, the amount of data is increased by a factor of three for a 3-axis geophone system. As this is an important consideration, it is desirable to consider in detail the performance gains that may be obtained.



II.2 Some Array Processing Fundamentals

A planar array processing problem shall be considered which has the following general description. The N sensors of the array are assumed to be located in the horizontal (i.e., x - y) plane with the i^{th} sensor located at the distance $\underline{r}_i^T \triangleq r_i(\cos \theta_i, \sin \theta_i, 0)^T$ from the origin. The magnitude of the distance is r_i and the angle θ_i is measured counterclockwise from the x -axis. The unit vector $\underline{\beta}$ defines the direction of motion of the incoming wave front that represents the signal. As indicated above, this vector can be defined in terms of the cone angle φ , $0 \leq \varphi \leq 90^\circ$, and the azimuth angle, $0 \leq \theta \leq 360^\circ$.

$$\underline{\beta} = \begin{pmatrix} \cos \theta \sin \varphi \\ \sin \theta \sin \varphi \\ \cos \varphi \end{pmatrix}; \quad \underline{\beta}^T \underline{\beta} = 1.$$

The speed of the wavefront is represented by c .

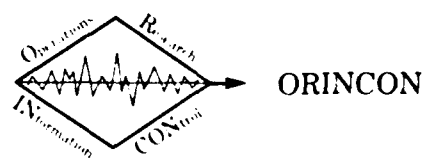
For the purposes of discussion, it is useful to reference the output of each sensor to the time at which the wave passes the origin of the coordinate frame. The signal that appears at the i^{th} sensor shall be regarded as the replica of the signal that would have been sensed at the origin except for a time shift τ_i given by

$$\tau_i = -\frac{\underline{\beta}^T \underline{r}_i}{c}. \quad (2.7)$$

Thus, the noise-free output of the i^{th} sensor can be written as

$$s_i(t) = s(t + \tau_i); \quad i = 1, 2, \dots, N \quad (2.8)$$

where $s(t)$ represents the time history of the signal appearing at the origin.



By introducing the time shifts τ_i for each i , $i = 1, 2, \dots, N$, the signals obtained from each sensor can be time-aligned since

$$s_i(t - \tau_i) = s(t), \quad i = 1, 2, \dots, N.$$

Then, by adding the time-delayed versions of the output, the signal is enhanced

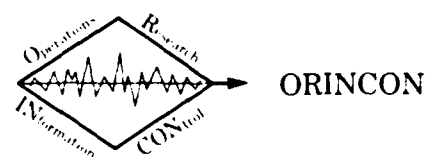
$$\sum_{i=1}^N s_i(t - \tau_i) = \sum_{i=1}^N s(t) = N s(t).$$

This simple observation forms the basis for array processing.

For seismic surveillance, the direction and speed of the incoming wave are unknown. Then, one can select a value for β and for c in order to define the time-delay τ_i , $i = 1, 2, \dots, N$. By delaying and summing the sensor outputs, a "beam" is formed in the selected direction and tests can be defined to detect the existence or absence of a signal emanating from the direction β . This concept forms the basis, either implicitly or explicitly, for any array processing scheme that is used for seismic surveillance. In the following paragraphs, the implications of this simple model are explored further in an effort to motivate the algorithmic approach stated in Part III.

The output $z_i(t)$ of the i^{th} sensor is described by (2.4). Suppose that estimates $\hat{\beta}$, \hat{c} of the signal direction and the wave speed are selected and used to define delays $\hat{\tau}_i$. Summing the delayed outputs, one obtains an estimate of the signal wave from

$$\begin{aligned} \hat{s}(t) &\triangleq \frac{1}{N} \sum_{i=1}^N z_i(t - \hat{\tau}_i) \\ &= \frac{1}{N} \sum_{i=1}^N s_i(t - \hat{\tau}_i) + \frac{1}{N} \sum_{i=1}^N n_i(t - \hat{\tau}_i). \end{aligned} \quad (2.9)$$



Clearly, if $\hat{\tau}_i = \tau_i$, the estimator assumes the form

$$\hat{s}(t) = s(t) + \frac{1}{N} \sum_{i=1}^N n_i(t - \hat{\tau}_i).$$

The coherent component of $n_i(t)$ is assumed to emanate from a different direction than $s(t)$ with the result that the $n_i(t)$ add with different phases and tend to cancel. The summation of the N sensor outputs tends to reduce the influence of the incoherent noise. Thus, the signal $s(t)$ should be enhanced relative to the noise. On the other hand, when $\hat{\tau}_i \neq \tau_i$, the signals also tend to cancel with the result that the signal estimate should indicate an absence of signal power relative to the noise.

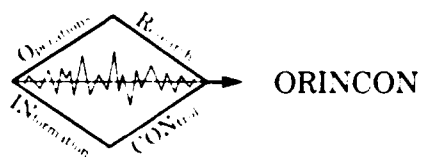
II.2.1 Response of a Beam-formed Array

The preceding discussion has shown that the signal is enhanced when its direction of arrival and wave speed correspond to the estimates of $\underline{\beta}$ and c . Consider the response of the beam-formed array to signals that arrive from an arbitrary direction $\underline{\beta}$ with a speed c . To simplify this analysis, only directional signals shall be considered and the response of the array to these signals shall be investigated.

Suppose that the sensor outputs $s_i(t)$ are delayed by $\hat{\tau}_i$ but a wave comes from a direction $\underline{\beta}$ with speed c . Thus, for signal alignment, the outputs would have to be delayed by τ_i . In this case

$$\begin{aligned} \hat{s}(t) &= \sum_{i=1}^N s_i(t - \hat{\tau}_i) \\ &= \sum_{i=1}^N s(t + \tau_i - \hat{\tau}_i) \end{aligned} \quad (2.10)$$

where



$$\tau_i - \hat{\tau}_i = -\frac{\underline{\beta}^T \underline{r}_i}{c} + \frac{\hat{\beta}^T \underline{r}_i}{c} = \left[\frac{\hat{\beta}}{c} - \frac{\underline{\beta}}{c} \right]^T \underline{r}_i$$

$$\Delta = -\underline{\beta}^T \underline{r}_i.$$

To facilitate the analysis, suppose that the signal has a Fourier transform so that

$$s(t) = \frac{1}{2\pi} \int_{-\infty}^{\infty} S(\omega) e^{j\omega t} d\omega$$

where $S(\omega)$ represents the Fourier transform of $s(t)$. For a time-delayed signal, this is written as

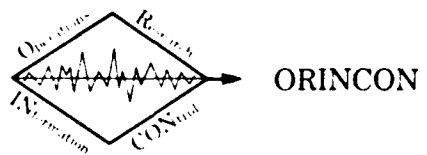
$$s(t - \Delta_i) = \frac{1}{2\pi} \int_{-\infty}^{\infty} S(\omega) e^{j\omega(t - \Delta_i)} d\omega.$$

Consequently, it follows that

$$\begin{aligned} \hat{s}(t) &= \sum_{i=1}^N s(t - \underline{\beta}^T \underline{r}_i) \\ &= \frac{1}{2\pi} \int_{-\infty}^{\infty} S(\omega) A(\omega, \underline{\beta}) e^{j\omega t} d\omega \end{aligned} \quad (2.11)$$

where

$$A(\omega, \underline{\beta}) = \sum_{i=1}^N e^{-j\omega \underline{\beta}^T \underline{r}_i}. \quad (2.12)$$



The quantity $A(\omega, \underline{v})$ is called the array pattern and is seen to depend upon the frequency and the wave characteristics as described by \underline{v} . A more general definition of the array pattern will be introduced subsequently. The quantity

$$\underline{k} \triangleq \frac{\omega \underline{\beta}}{c}$$

is called the wave number vector and has the units of inverse distance. Note also that the wave length is defined as

$$\lambda = 2\pi \frac{c}{\omega}.$$

Examination of (2.11) indicates that $A(\omega, \underline{v})$ serves as a filter operating on the signal spectrum $S(\omega)$. That is, $s(t)$ is represented as the Fourier transform of the product of $S(\omega)$ and $A(\omega, \underline{v})$. Consequently, the influence of the incoming signal on the array response is established by investigating the properties of the array pattern.

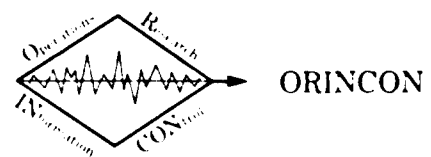
If the signal is narrowband with center frequency ω_c , the behavior of $A(\omega_c, \underline{v})$ as a function of \underline{v} determines the array response. Obviously, if $\underline{\beta}/c = \underline{\beta}/c$, then $\underline{v} = 0$ and it follows that for any frequency

$$A(\omega, 0) = N.$$

This observation reconfirms the signal enhancement property of the array when the sensor outputs are aligned. Nonzero values of \underline{v} indicate the frequency-dependent response of the array.

II.2.2 Linear Array Response

Much of the published literature [e.g., see References 6, 7 or 8] dealing with arrays is based on specific array configurations whose geometry is chosen to simplify the analysis and to gain useful insights into the array response. To illustrate the frequency response determination in a closed form, it is useful to consider a linear array with equidistant sensors at a spacing D . Assume that the first sensor is located at the origin of the coordinate system (i.e., $r_i = 0$) and suppose that



the remaining ($N-1$) sensors are positioned along the positive x -axis.
Then, it follows that

$$\underline{r}_i = iD \underline{i}_x$$

where \underline{i}_x denotes the unit vector defining the x -axis. Suppose further that only the horizontal wave motion is considered so that

$$\begin{aligned} \tau_i &= -\frac{\underline{s}^T \underline{r}_i}{c} \\ &= \frac{iD}{c} \underline{s}^T \underline{i}_x \\ &= -\frac{iD}{c} \cos \theta. \end{aligned}$$

Similarly, it follows that

$$\hat{\tau}_i = -\frac{iD}{\hat{c}} \cos \hat{\theta}.$$

For this planar situation, the array pattern assumes the form

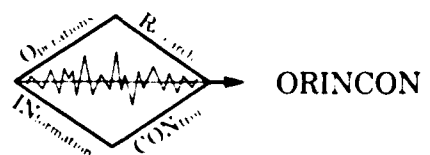
$$A(\omega, \underline{v}) = \sum_{i=1}^N e^{-jD \left(\frac{\cos \hat{\theta}}{\hat{c}} - \frac{\cos \theta}{c} \right) \omega}.$$

Let

$$\eta \triangleq D \left(\frac{\cos \hat{\theta}}{\hat{c}} - \frac{\cos \theta}{c} \right) \omega$$

so

$$A(\eta) \triangleq \sum_{i=1}^N e^{-j\eta i}.$$



But the summation can be expressed as

$$\begin{aligned}
 A(\eta) &= e^{-j\eta} \left(\frac{1 - e^{-jN\eta}}{1 - e^{-j\eta}} \right) \\
 &= \left| \frac{\sin(N\eta/2)}{\sin(\eta/2)} \right| e^{-j \frac{(N+1)\eta}{2}}. \tag{2.13}
 \end{aligned}$$

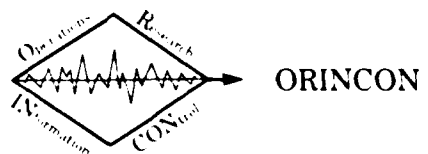
The array pattern $A(\eta)$ is periodic with period $\eta = 2\pi$. The maxima occur at $\eta = 2n\pi$, $n \in 0, \pm 1, \pm 2, \dots$. The maximum that occurs at $\eta = 0$ is referred to as the mainlobe and

$$\left| \frac{\sin(N\eta/2)}{\sin(\eta/2)} \right|_{\eta=0} = N.$$

The other maxima for $n \neq 0$ define the grating lobes of the array and are undesirable as they imply that signals with directions that generate these values of η are enhanced as much as signals with direction $\hat{\beta}$ and speed c . The array pattern vanishes for $\eta = 2\pi m/N$, $m = \pm 1, \pm 2, \dots, \pm(N-1)$ to form nulls. Waves corresponding to these nulls are attenuated totally for some frequency.

The mainlobe occurs at $\eta = 0$ and the grating lobes are located at $\eta = \pm 2\pi, \pm 4\pi, \dots$. It is desirable to avoid the influence of the grating lobes since signals with characteristics that yield values of η corresponding to the location of the grating lobes are enhanced. The grating lobes can be eliminated for band limited signals through the appropriate choice of the sensor spacing D.

Suppose η_b defines the highest possible frequency of the signal. Then, for waves such that $c = \hat{c}$, the variable η can be rewritten as



$$\begin{aligned}
 n &= D(\cos \hat{\theta} - \cos \theta) \omega / c \\
 &\leq D(\cos \hat{\theta} - \cos \theta) \omega_B / c \\
 &= 2\pi (\cos \hat{\theta} - \cos \theta) D / \lambda_B
 \end{aligned}$$

where

$$\lambda_B \triangleq 2\pi c / \omega_B.$$

To eliminate the grating lobes, n should be restricted to a magnitude less than 2π

$$|n| \leq 2\pi.$$

This can be achieved for any angles $\hat{\theta}, \theta$ by choosing the sensor spacing such that

$$D \leq \lambda_B / 2.$$

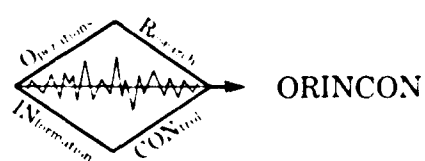
This requirement represents the spatial version of the well-known sampling theorem. λ_B represents the shortest wavelength present in the incoming signal. Thus, there should be at least two sensors contained in the interval defined by λ_B .

It is useful to continue the analysis for some examples. Suppose that a broadside beam is considered (i.e., $\hat{\theta} = \pi/2$) for $D/\lambda_B = 1/2$. Then it follows that

$$-\pi \leq n \leq \pi.$$

For an endfire beam (i.e., $\hat{\theta} = 0$), one sees that

$$0 \leq n \leq 2\pi.$$



Nulls in the array pattern occur for $\eta = 2\pi m/N$; $m = \pm 1, \pm 2, \dots, \pm(N-1)$. The location of the null depends upon the wavelength, the array spacing, the number of sensors, and the direction of arrival of the wave. For a broadside beam and minimal spacing $D = \lambda_B/2$, the first null occurs at $\eta = \pm 2\pi/N$ so

$$\cos \theta_1 = 2/N.$$

Since the maximum occurs at $\theta = \pi/2$, the width of the mainlobe as measured by the distance between the first nulls is

$$BW = 2(\pi/2 - \theta_1).$$

This provides a convenient measure of the beamwidth of the array. Note that for large N , this beamwidth is given approximately by

$$BW \approx 4/N.$$

Thus, the beamwidth is proportional to the number of sensors for the fixed spacing $D = \lambda_B/2$. For an arbitrary spacing D , the first null occurs at

$$\cos \theta_1 \approx \frac{\lambda}{ND}$$

and induces the beamwidth for large N of

$$BW = \frac{2\lambda}{ND}.$$

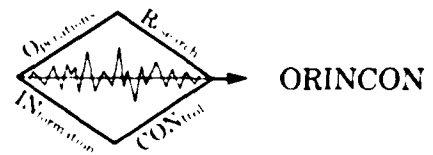
Thus, the beamwidth is a function of the length of the array rather than the number of sensors.

For endfire beams, the first null occurs at

$$\frac{2\pi}{N} = (1 - \cos \theta_1) \frac{2\pi D}{\lambda}$$

or

$$\cos \theta_1 = 1 - \frac{\lambda}{ND}$$



and the resulting beamwidth is

$$BW = 2\theta_1.$$

For small λ/ND , this reduces approximately to

$$\theta_1 \approx \sqrt{\frac{2\lambda}{ND}}.$$

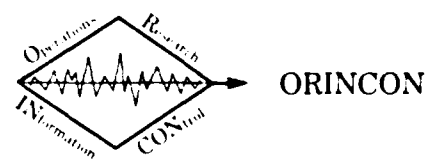
Now, the beamwidth is inversely proportional to the square root of the array length.

Another measure of the array capability is provided by determining the magnitude of the sidelobes relative to the magnitude of the mainlobe. It can be shown for large N that the magnitude $|A_1|$ of the first sidelobe to the magnitude $|A_0|$ of the mainlobe is approximately

$$\frac{|A_1|}{|A_0|} \approx \frac{2}{3\pi}.$$

Thus, the sidelobe magnitude is approximately 13.5 dB less than the mainlobe. To first order, this ratio is not affected by the array length nor by the number of sensors.

The linear array produces an array pattern that depends upon the beam direction $\hat{\theta}$. If the signal direction is not known, it may be desirable to consider array configurations that exhibit angular symmetry. In this case, circular arrays may be more suitable. The analysis of a circular array is considerably more complicated than for a linear array (e.g., see Ma [7]) and shall not be presented here. However, for any array configuration, the array pattern can be studied numerically by returning to the defining relation (2.12). For a small array (i.e., $N \leq 20$) the calculations are not lengthy. For a planar array, the graphical presentation of the numerical results is more complicated. We shall return to this point in Part III.

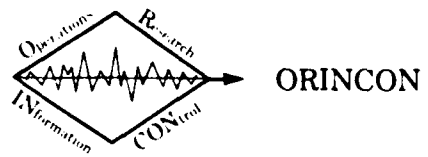


Let us summarize and generalize the important points of the discussion of linear arrays.

1. The magnitude of the array pattern provides the basic characterization of the array response. Because of the polynomial character of the array pattern, it is useful to investigate the maxima and minima of $|A(\omega, \underline{v})|$.
2. The maximum of $|A(\omega, \underline{v})|$ is achieved for $\underline{v} = 0$. However, maxima of equal magnitude can be experienced for other values of \underline{v} . The influence of these grating lobes can be eliminated through the sensor spacing.
3. Grating lobes can also be avoided by using nonuniform spacings of array elements. The uniform spacing of elements is often introduced more for the convenience of the analyst than for any other defensible reason. Nonuniform spacings may be more appropriate when some prior knowledge of beam direction is available.
4. The resolution of the array is measured primarily by the width of the main lobe and by the ratio of the mainlobe and sidelobe magnitudes. For the example, the width of this lobe is inversely proportional to the length of the array. The relative magnitudes are independent of the number of sensors.
5. As discussed below, the array resolution can be modified for an array of fixed dimension through the introduction of weights for the sensor outputs or through the nonuniform spacing of the sensor elements.
6. An important indicator of the discrimination capability of the array is obtained by comparing the magnitude of the mainlobe with the sidelobe magnitudes. The array effectiveness can be regarded as improving as the ratio of the magnitude increases. The directivity is a quality that is intended to serve as a measure of effectiveness and is defined below.

The number of sensors N serves to introduce limitations regarding the processing gain that is possible for an array. The array geometry can be chosen to provide maximal gain for a given number of sensors. As indicated above, linear or even circular arrays with uniform element spacings do not necessarily provide the optimal configuration. However, these uniform configurations do have the advantages of convenience. Even for uniform arrays, processing gains are possible relative to the simple delay and sum configurations introduced above by introducing weights w_i for the output of each sensor element.

For seismic surveillance, the number of sensors in an array can be expected to be relatively small. As a result, attention must be directed to the extraction of a maximal amount of information from the sensor data. This requires a careful definition of the array performance measure, of the system description, and of the class of admissible processing algorithms. It is to these questions that the following discussion is addressed.



II.3 The Array Processing Problem and Array Directivity

The array processing problem can be defined in the context of a parameter and signal estimation problem and this approach is taken and developed here. Basically, we shall consider the estimation of $s(t)$, β and c from the sensor output $z_i(t)$, $i = 1, 2, \dots, N$. It is assumed that the estimator is restricted to the general form

$$\hat{s}(t) = \sum_{i=1}^N w_i z_i(t-\tau_i) \quad (2.14)$$

where the delays τ_i are selected to estimate the direction β and speed c of the incoming wavefront. The weights w_i are used to improve the ability of the array to discriminate between signals from nearly equal direction with similar speeds. Imbedded in the delays τ_i are the sensor locations. The array configuration can also be adjusted to enhance the performance of the array.

As indicated in (2.14), the estimator $\hat{s}(t)$ is formed as a linear combination of the time-delayed sensor outputs. For generality, one could consider complex weights operating on the complex representation of the output signal in (2.14). This shall not be done here although the extension of the following results for real weights and real output signals is simple [e.g., see Reference 8]. It involves primarily a modest change in notation.

The estimator in (2.14) can be written in vector notation as

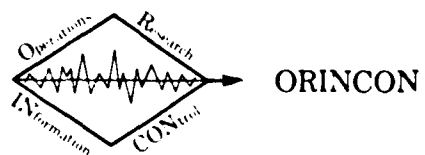
$$\hat{s}(t) = \underline{w}^T \underline{x}(t) \quad (2.15)$$

where

$$\underline{w}^T \triangleq (w_1, w_2, \dots, w_N)$$

$$\underline{x}(t) \triangleq (z_1(t-\tau_1), z_2(t-\tau_2), \dots, z_N(t-\tau_N))$$

$$\triangleq (x_1(t), x_2(t), \dots, x_N(t)).$$



Wherever possible, summation notation, as used in (2.14), will be replaced with more compact vector notation introduced in (2.15). The equivalence of the two representations is apparent.

The sensor output $z_i(t)$ is defined to have the form

$$z_i(t) = s_i(t) + n_i(t).$$

If τ_i represents the actual signal delay, then

$$\begin{aligned} z_i(t-\tau_i) &= s_i(t-\tau_i) + n_i(t-\tau_i) \\ &= s(t) + n_i(t-\tau_i) \\ &\triangleq x_i(t). \end{aligned}$$

The collection of all N sensor outputs can be expressed in vector form as

$$\underline{x}(t) = s(t) \underline{1} + \underline{n}'(t) \quad (2.16)$$

where

$$\underline{1}^T \triangleq (1, 1, \dots, 1)^T$$

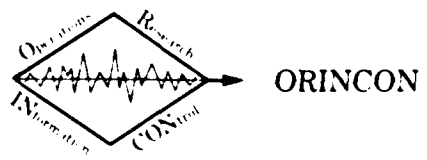
and

$$\underline{n}'^T(t) \triangleq (n_1(t-\tau_1), n_2(t-\tau_2), \dots, n_N(t-\tau_N))^T.$$

Equation (2.16) defines the signal-aligned (or beam-formed) statement of the problem. Using (2.15), it follows that

$$\begin{aligned} \hat{s}(t) &= \underline{w}^T [s(t) \underline{1} + \underline{n}'(t)] \\ &= s(t) \left[\sum_{i=1}^N w_i \right] + \underline{w}^T \underline{n}'(t). \end{aligned}$$

It is reasonable to expect that $\hat{s}(t)$ should equal $s(t)$ in the absence of noise and other errors. This implies that the weights should satisfy the normalization condition.



$$\sum_{i=1}^N w_i = \underline{w}^T \underline{1} = 1. \quad (2.17)$$

For example, uniform weights, $w_i = w_j$ for all i, j , must be

$$w_i = 1/N.$$

We shall return to the signal-aligned model (2.16) during the subsequent model. First, we shall examine basic properties of the array as implied by (2.15).

II.3.1 The General Array Pattern

Suppose that the sensor outputs are delayed by $\hat{\tau}_i$

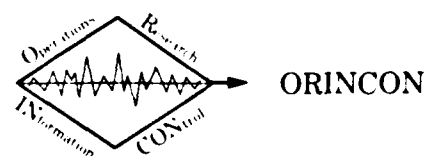
$$\hat{\tau}_i = -\frac{\underline{\beta}^T \underline{r}_i}{\hat{c}}$$

where $\hat{\beta}$ and \hat{c} represent estimates of the wave front direction and speed. Then, for signals with direction $\underline{\beta}$ and speed c , the array output is given by

$$\begin{aligned} \hat{s}(t) &= \sum_{i=1}^N w_i s_i(t - \hat{\tau}_i) \\ &= \sum_{i=1}^N w_i s(t - \hat{\tau}_i + \tau_i) \\ &= \sum_{i=1}^N w_i s(t - \underline{v}^T \underline{r}_i) \end{aligned}$$

where

$$\underline{v} = -\left[\frac{\hat{\beta}}{\hat{c}} - \frac{\underline{\beta}}{c} \right].$$



Assuming, as above, that the signal has a Fourier transform, this can be rewritten as

$$\hat{s}(t) = \frac{1}{2\pi} \int_{-\infty}^{\infty} S(\omega) A(\omega, \underline{v}, \underline{w}) e^{j\omega t} d\omega \quad (2.18)$$

where

$$A(\omega, \underline{v}, \underline{w}) \triangleq \sum_{i=1}^N w_i e^{-j\omega v^T r_i} \quad . \quad (2.19)$$

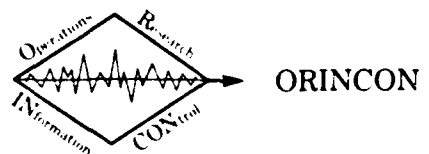
The quantity $A(\omega, \underline{v}, \underline{w})$ is defined as the array pattern and has the same form introduced in (2.12) with the addition of the weighting vector \underline{w} . It should be emphasized that (2.19) is valid for any weight vector that satisfies (2.17).

Considerable information is provided from the analysis of the array pattern. It is convenient to rewrite the exponent in (2.19) in terms of the angular variables defining the arrival directions. Note that since the sensors are assumed to be contained in the x-y plane the sensor location can be expressed as

$$\underline{r}_i = r_i \begin{pmatrix} \cos \theta_i \\ \sin \theta_i \\ 0 \end{pmatrix} \quad .$$

Also, the arrival direction β can be written in terms of the cone and azimuth angles as

$$\underline{\beta} = \begin{pmatrix} \cos \psi \sin \varphi \\ \sin \psi \sin \varphi \\ \cos \varphi \end{pmatrix} \quad .$$



Then, we see that

$$\begin{aligned}\omega \underline{\underline{\beta}}^T \underline{r}_i &= \omega \left(\frac{\hat{\underline{\beta}}}{\hat{c}} - \frac{\underline{\beta}}{c} \right)^T \underline{r}_i \\ &= \omega \left[\frac{\hat{\underline{\beta}}^T \underline{r}_i}{\hat{c}} - \frac{\underline{\beta}^T \underline{r}_i}{c} \right] \\ &\triangleq \psi_i - \frac{2\pi}{\lambda} \underline{\underline{\beta}}^T \underline{r}_i = \psi_i - k \underline{\underline{\beta}}^T \underline{r}_i\end{aligned}$$

where

$$\psi_i \triangleq \frac{2\pi}{\lambda} \hat{\underline{\beta}}^T \underline{r}_i = \hat{k} \hat{\underline{\beta}}^T \underline{r}_i$$

$$\lambda = \frac{2\pi c}{\omega}$$

and

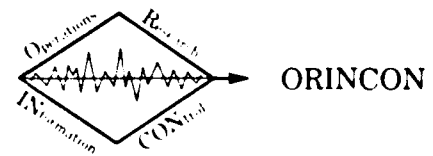
$$k \triangleq \frac{v}{c} = \text{wave number}.$$

But it follows that

$$\underline{\underline{\beta}}^T \underline{r}_i = r_i \sin \varphi \cos(\theta - \theta_i).$$

It is useful to consider the array pattern as a function of the arrival angles θ, φ for fixed frequencies ω , sensor locations \underline{r}_i , and array parameters $\hat{\underline{\beta}}, \hat{c}, \underline{w}$. Thus, it becomes convenient to define

$$A(\omega, \underline{\underline{\beta}}, \underline{r}_i) \triangleq A(\theta, \varphi)$$



and note from the preceding discussion that

$$A(\theta, \varphi) = \sum_{i=1}^N w_i e^{-j[\psi_i - k r_i \sin \varphi \cos(\theta - \theta_i)]} \quad (2.20)$$

A specific array configuration defines r_i and θ_i . The weights can be determined from a variety of arguments such as presented below.

The angle ψ_i is defined in terms of r_i , θ_i , $\hat{\theta}$, $\hat{\varphi}$ and \hat{k} . The wave numbers, k and \hat{k} , depend upon the signal frequency. For a narrow-band frequency, the center frequency represents the single frequency of interest. By assigning values to all of these physical parameters, the magnitude

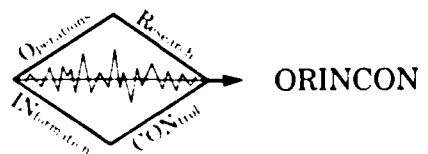
$$|A(\theta, \varphi)|^2 = A(\theta, \varphi)A^*(\theta, \varphi)$$

can be determined to establish the array response to signals emanating from directions (θ, φ) . This computation should be regarded as fundamental to the analysis of any array processor.

II.3.2 Optimal Array Directivity

Suppose that one wants the array to be as sensitive as possible in the mainbeam direction relative to the average of the sensitivity in all other directions. This represents a reasonable objective when there is no information available regarding the direction of potential interference sources. One can formulate this problem quantitatively in the following manner.

The array pattern magnitude-squared $|A(\theta, \varphi)|^2$ describes the response of the beam-formed array to signals coming from the direction θ, φ . The average response is obtained by integrating with respect to all possible values of θ, φ .



$$\text{Average response} \triangleq \frac{1}{2\pi} \int_0^{2\pi} d\theta \int_0^{\pi/2} |A(\theta, \varphi)|^2 g(\theta, \varphi) \sin \varphi d\varphi. \quad (2.21)$$

In (2.21), we assume that the cone angle φ is equally likely for $0 \leq \varphi \leq \pi/2$ and arrivals from above the earth (i.e., $\pi/2 \leq \varphi \leq \pi$) are impossible. The weighting $g(\theta, \varphi)$ is included to indicate sensor limitations. For example, a vertical seismometer cannot sense horizontal particle motions but is otherwise isotropic. Then, one might choose $g(\theta, \varphi) = \cos \varphi$ to reflect this sensitivity.

The directivity of the array for an arbitrary direction (θ_o, φ_o) is defined as

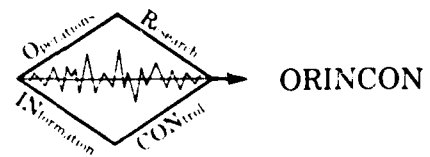
$$D \triangleq \frac{|A(\theta_o, \varphi_o)|^2}{\frac{1}{2\pi} \int_0^{2\pi} d\theta \int_0^{\pi/2} |A(\theta, \varphi)|^2 g(\theta, \varphi) \sin \varphi d\varphi}. \quad (2.22)$$

D indicates the sensitivity in the direction (θ_o, φ_o) relative to the average sensitivity in all directions. A general problem can be stated in the following manner.

Maximum Directivity: Choose the weights w_i and the phases ψ_i to maximize D for the direction (θ_o, φ_o) .

Basically, this problem statement assumes the use of complex weights with amplitudes w_i and phases ψ_i . For our purposes, we have chosen the phases ψ_i by defining $\hat{\theta}, \hat{\varphi}$. Furthermore, we want to maximize the directivity for

$$\hat{\varphi} = \varphi_o, \quad \hat{\theta} = \theta_o.$$



In this case,

$$\begin{aligned} A(\hat{\theta}, \hat{\varphi}) &= \sum_{i=1}^N w_i e^{-j(\hat{k}-k)r_i \sin \hat{\varphi} \cos(\hat{\theta}-\theta_i)} \\ &= 1 \text{ if } k = \hat{k} \end{aligned}$$

To proceed, define the vector \underline{b} as

$$\underline{b}^T \triangleq [w_1 e^{-j\psi_1}, \dots, w_N e^{-j\psi_N}] \quad (2.23a)$$

and let \underline{g} be

$$\underline{g}^T \triangleq [e^{jkr_1 \sin \varphi \cos(\theta-\theta_1)}, \dots, e^{jkr_N \sin \varphi \cos(\theta-\theta_N)}] \quad (2.23b)$$

With these definitions,

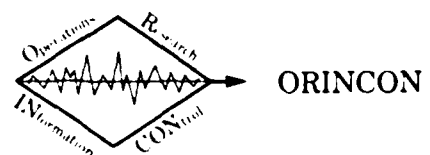
$$A(\theta, \varphi) = \underline{b}^T \underline{g}$$

and

$$\begin{aligned} |A(\theta, \varphi)|^2 &= (\underline{b}^T \underline{g})^* (\underline{b}^T \underline{g}) \\ &= \underline{b}^{*T} \underline{g}^* \underline{g}^T \underline{b} \\ &\triangleq \underline{b}^{*T} G \underline{b} \end{aligned}$$

where $(\cdot)^*$ represents the complex conjugate of (\cdot) . Since \underline{b} does not depend upon θ or φ , it follows that

$$\begin{aligned} D_{AV} &\triangleq \frac{1}{2\pi} \int_0^{2\pi} d\theta \int_0^{\pi/2} |A(\theta, \varphi)|^2 g(\theta, \varphi) \sin \varphi d\varphi \\ &= \underline{b}^{*T} B \underline{b} \end{aligned}$$



where

$$B \triangleq \frac{1}{2\pi} \int_0^{2\pi} d\theta \int_0^{\pi/2} g(\theta, \varphi) [\underline{g}^* \underline{g}^T] \sin \varphi d\varphi .$$

Thus, the directivity for any θ_o, φ_o has the form

$$D = \frac{\underline{b}^* \underline{G}_o \underline{b}}{\underline{b}^* \underline{B} \underline{b}} \quad (2.24)$$

where

$$\underline{G}_o \triangleq \underline{g}_o^* \underline{g}_o^T$$

and

$$\underline{g}_o \triangleq \underline{g} \Big|_{(\theta_o, \varphi_o)}$$

The directivity D is maximized by choosing \underline{b} in (2.24) to maximize the ratio of two quadratic forms. It can be shown that the matrix B is positive-definite. Using results from matrix theory [9] (i.e., the Rayleigh quotient), the ratio is maximized when \underline{b} is the eigenvector satisfying

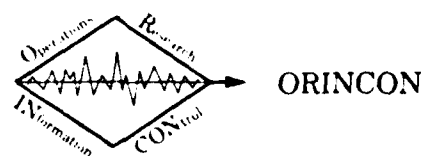
$$\underline{G}_o \underline{b}_M = \lambda_M \underline{B} \underline{b}_M$$

where λ_M is the largest eigenvalue of the regular pencil $(A - \lambda B)$.

When \underline{G}_o is formed as an outer product as in (2.24), the maximum eigenvalue is

$$\lambda_M = \underline{g}_o^* \underline{B}^{-1} \underline{g}_o$$

and the eigenvector corresponding to λ_M is



$$\underline{b}_M = B^{-1} \underline{g}_o .$$

Since we have defined the phase values ψ_i , the preceding results specialize in the following manner. Note that

$$A(\hat{\theta}, \hat{\varphi}) = \underline{b}^T \hat{\underline{g}}_o = \underline{w}^T \underline{l} .$$

This implies that

$$\begin{aligned} \underline{b}^{*T} \hat{G} \underline{b} &= \underline{b}^{*T} \hat{\underline{g}}^* \hat{\underline{g}}^T \underline{b} \\ &= \underline{w}^T \underline{l} \underline{l}^T \underline{w} \\ &= \underline{w}^T O \underline{w} . \end{aligned}$$

Further, it follows that

$$\underline{b} = \Psi \underline{w}$$

$$\text{where } \Psi \triangleq \text{diag}[e^{-j\psi_i}] .$$

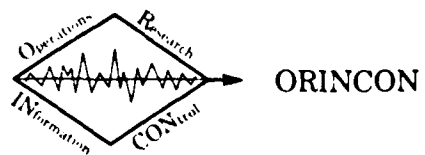
Consequently,

$$\underline{b}^{*T} B \underline{b} = \underline{w}^T \Psi^* T_B \Psi \underline{w} \triangleq \underline{w}^T C \underline{w}$$

where $C \triangleq \Psi^* T_B \Psi$. The directivity reduces to

$$D = \frac{\underline{w}^T O \underline{w}}{\underline{w}^T C \underline{w}} . \quad (2.25)$$

The matrix C is positive-definite since Ψ and B are positive-definite. Thus the preceding results apply and D has the maximum value



$$D_M = \underline{1}^T C^{-1} \underline{1} \quad (2.26a)$$

and

$$\underline{w}_M = C^{-1} \underline{1}. \quad (2.26b)$$

Thus, the gains that maximize the directivity of the array in the direction θ, φ are given by (2.26b). This calculation requires the determination of the matrix C and its inverse. For uniform linear or circular arrays, the calculation of B can be accomplished in a closed form [10]. The inversion of C can be computationally burdensome, particularly for large arrays, but it is conceptually straightforward.

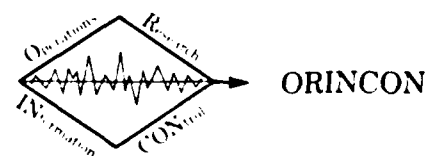
When there is no information regarding the noise field, the preceding discussion provides a reasonable approach to choosing the array weights \underline{w} . Simple examples demonstrate that considerable improvements are possible. For example, the directivity of a uniformly-spaced linear array with isotropic elements spaced at intervals of 0.425λ has a directivity of 12.5. Using optimal weights obtained by solving (2.26b), the directivity for this array is 22.0. Thus, D is increased almost by a factor of two.

II. 3.3 Null Placement and Maximum Directivity

The preceding approach can be extended to consider the case in which an interference signal emanates from a known direction (θ_I, φ_I) with speed c . To eliminate the influence of the interference signal, one can choose to locate a null of the array pattern in the direction (θ_I, φ_I) . This can be accomplished with only a modest change in the preceding result. Let \underline{g}_I define the vector associated with (θ_I, φ_I)

$$\underline{g}_I^T \triangleq [e^{jkr_i \sin \varphi_I \cos(\theta_I - \theta_1)}, \dots, e^{jkr_N \sin \varphi_I \cos(\theta_I - \theta_N)}].$$

To obtain a null in this direction, the weight vector \underline{b} is required to be orthogonal to \underline{g}_I since the array pattern magnitude vanishes.



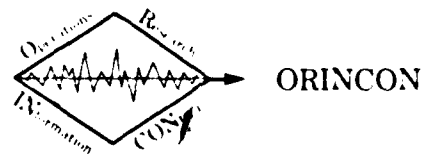
$$\underline{g}_I^{*T} \underline{b} = 0. \quad (2.27)$$

Now, we want to maximize D subject to the constraint (2.27). Note that as many as $(N-1)$ nulls can be introduced by defining constraints having the form (2.27). This is obvious since the N sensors cause the weight vector to be N-dimensional. An optimization problem can be defined when there are no more than $(N-1)$ constraints.

The presence of constraints (2.27) reduces the number of degrees of freedom available for the optimization. In general, the imposition of constraints means that the maximum directivity is less than can be achieved for the unconstrained problem. It has the effect that the optimization problem can be formulated in a lower-dimensional space. Effectively, the dimension of the matrix that must be inverted in (2.26) is smaller. This is accomplished by solving the M constraints for M variables in terms of the remaining $(N-M)$ variables. Then, these M variables are eliminated in the directivity equation to define an unconstrained maximization problem involving $(N-M)$ variables. Because the constraints are linear, the nature of the original problem is not altered. One is still concerned with maximizing the ratio of two quadratic forms.

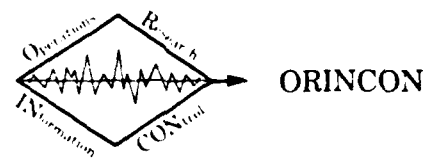
Let us summarize the preceding discussion.

- (1) The weights of the estimator (2.15) can be selected to maximize the directivity (2.22). The optimal weights are obtained from (2.26) and requires the inversion of an $(N \times N)$, positive-definite matrix.
- (2) As we shall see below, the general structure of the optimal solution as given by (2.26) repeats for other problem formulations.
- (3) Nulls can be imposed in the direction of as many as $(N-1)$ known interference sources. The imposition of these constraints does not alter the form of the optimal



solution other than to reduce the dimensionality of the optimization problem.

- (4) The problem that has been formulated requires almost no information regarding the nature of the signal and noise. However, the calculation of the average response (2.21) can be interpreted as assuming that the noise is uniformly distributed for $0 \leq \theta \leq 2\pi$, $0 \leq \theta \leq \pi/2$. Nonetheless, this approach can be regarded as utilizing a minimal number of assumptions regarding the structure of the signal and noise.



II.4 A Statistical Approach to Optimal Array Processing

The signal-aligned model of the problem was given in (2.16). This model shall be used as the basis for the remaining discussion in which we shall introduce statistical descriptions for the noise to obtain optimal estimation and detection algorithms.

Consider the noise $\underline{n}'(t)$. During any time interval, it is unrealistic to expect that the output noise will be known or predictable. A stochastic model is indicated and $\underline{n}'(t)$ shall be regarded as a realization of a random process. For a limited time interval, it is reasonable to assume that $\underline{n}'(t)$ is a stationary random process with zero mean.

$$E[\underline{n}'(t)] = 0 \quad \text{for all } t .$$

The assumption of zero mean can be justified since the noise basically is composed of a combination of seismic waves from many unknown sources and electronic sensor noise. If the sensors are calibrated adequately, the sensor noise should have zero mean.

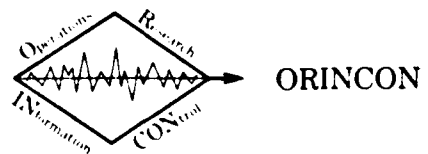
The second-order statistics for the noise must also be specified. For the i^{th} sensor, the correlation of the output noise is given by

$$r_n^{ii}(\Delta) \triangleq E[n_i(t) n_i(t-\Delta)].$$

The cross-correlation of the noise in the i^{th} and j^{th} sensors is

$$r_n^{ij}(\Delta) \triangleq E[n_i(t) n_j(t-\Delta)].$$

Thus, the correlation matrix for the noise vector is an $(N \times N)$ matrix with elements $r_n^{ij}(\Delta)$.



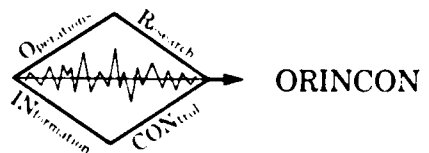
$$R_{n'}(\Delta) = E[\underline{n}'(t)\underline{n}'^T(t-\Delta)]$$

$$= \left\{ r_n^{ij}(\Delta + \tau_j - \tau_i) \right\}$$

where τ_i represents the delay associated with the i^{th} sensor as defined above. It is assumed that $R_{n'}(\Delta)$ is either known or can be determined. Then, optimal array processing algorithms can be defined for estimating and/or detecting the signal.

In general, the noise can be regarded as arising from either the electronics of the sensor or from seismic sources. Electronic sensor noise can be expected to be statistically independent from sensor to sensor, thereby inducing a spatial "white noise." Furthermore, it is reasonable to assume that this type of noise is temporally white (i.e., broadband relative to the range of frequencies important for seismic signal processing). In addition to the electronic noise, the sensor output can be expected to reflect noise signals generated from unknown seismic sources. Background noise from a number of distant sources may combine to produce outputs that appear to have no directional characteristics that induce a spatial independence among the sensor outputs. However, it is realistic to expect that some directional noise sources will appear in the sensor outputs that will produce correlation among the sensor outputs. Commonly, these directional noise signals represent the greatest source of difficulty for the signal processor. Their influence must be eliminated to enhance the ability of the signal processor to detect signals emanating from specific directions.

Two types of directional noise can be considered. In some cases the direction of the noise is known. Then, the signal processor attempts to place a null of the array pattern in the known noise



direction in order to eliminate its influence. In many other cases, the existence and location of a directional source is unknown. Then, the signal processor should adapt to recognize and to eliminate the effects of a noise source having these unknown characteristics.

II.4.1 The Linear, Minimum Mean-Square Error Estimator

To begin the development of array signal processing algorithms, suppose that the noise covariance matrix R_n' is known. Later, we shall consider the more realistic case in which R_n' must be estimated. Suppose that the signal $s(t)$ is assumed to be deterministic but completely unknown. Let us assume that $s(t)$ is to be estimated as a linear combination of the delayed sensor outputs $\underline{x}(t)$. Thus,

$$\hat{s}(t) \triangleq \underline{w}^T \underline{x}(t)$$

where $\underline{w} \triangleq (w_1, w_2, \dots, w_N)^T$.

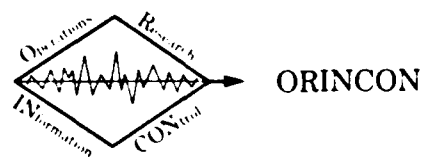
Let us require that this estimator is absolutely unbiased [11]. That is, we want the conditional expectation to equal the signal.

$$E[\hat{s}(t) | s(t)] = s(t).$$

To achieve this requirement, note that

$$\begin{aligned} E[\hat{s}(t) | s(t)] &= E[\underline{w}^T \underline{x}(t) | s(t)] \\ &= \underline{w}^T E[\underline{x}(t) | s(t)] \\ &= \underline{w}^T [s(t) \underline{1}] \end{aligned}$$

since $E[\underline{n}'(t)] = 0$. But this reduces to



$$E[\hat{s}(t)|s(t)] = \left[\sum_{i=1}^N w_i \right] s(t) .$$

Consequently, an unbiased estimator is obtained by requiring that

$$\sum_{i=1}^N w_i = 1 .$$

Observe that uniform weighting

$$w_i = 1/N, \quad i = 1, 2, \dots, N$$

yields an unbiased estimator and confirms the earlier discussion.

Suppose that the weights w are chosen to minimize the mean-square error in the estimation. That is, choose w so that

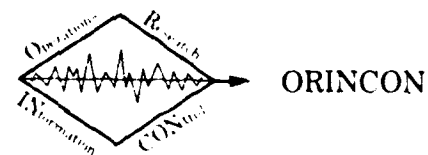
$$\lambda_{AMS} = E[(s(t) - \hat{s}(t))^2 | s(t)] \quad (2.28)$$

is minimized. The Gauss-Markov Theorem [e.g., see Reference 11] asserts that the absolutely unbiased, linear, minimum mean-square estimator of s is given by

$$\begin{aligned} \hat{s}_{AMS}(t) &= \frac{\underline{1}^T R_n^{-1}}{\underline{1}^T R_n^{-1} \underline{1}} \underline{x}(t) \\ \hat{s}_{AMS}(t) &\triangleq w_{AMS}^T \underline{x}(t). \end{aligned} \quad (2.29)$$

The variance σ_s^2 of the error in this estimator is given by

$$\begin{aligned} \sigma_s^2 &\triangleq E[(s - \hat{s})^2 | s] \\ &= (\underline{1}^T R_n^{-1} \underline{1})^{-1}. \end{aligned}$$



Let us compare the optimal weight \underline{w}_{AMS} with the weight \underline{w}_M that maximizes the array directivity.

$$\underline{w}_{AMS} = \frac{\underline{1}^T \underline{R}_{n'}^{-1} \underline{1}}{\underline{1}^T \underline{R}_{n'}^{-1} \underline{1}} \underline{R}_{n'}^{-1} \underline{1}$$

$$\underline{w}_M = C^{-1} \underline{1} .$$

Both gains require the inversion of an ($N \times N$) matrix. The matrix C is related to the average of the magnitude-squared array pattern. Consequently, it permits an interpretation that has some characteristics in common with the noise covariance matrix $R_{n'}$. However, the matrices C and $R_{n'}$ are obtained in very different ways. The estimator (2.29) provides a conceptual flexibility that is very useful. In fact, (2.29) provides the basis for adaptive array processing in which the noise covariance $R_{n'}$ is estimated from the sensor data. By generating estimates of the noise covariance for use in the signal estimator, the processor can be regarded as adapting to the current environment. Thus, it is useful to examine the properties of the estimator (2.29) in greater detail.

Suppose, first, that $R_{n'}$ is a diagonal matrix (i.e., the noise is spatially and temporally white).

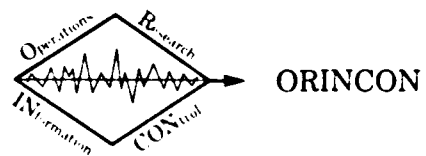
$$R_{n'} = \text{diag} \{r_n^{ii}(0)\} .$$

Then,

$$R_{n'}^{-1} = \text{diag} \{1/r_n^{ii}(0)\}$$

and it follows that

$$\underline{1}^T R_{n'}^{-1} = \left(-\frac{1}{r_n^{11}}, \frac{1}{r_n^{22}}, \dots, \frac{1}{r_n^{NN}} \right)$$



and

$$\underline{1}^T R_n^{-1} \underline{1} = \sum_{i=1}^N 1/r_n^{ii}.$$

Consequently, the estimator is given by

$$\hat{s}_{AMS}(t) = \frac{1}{\sigma_s^2} \sum_{i=1}^N x_i(t)/r_n^{ii}.$$

From this expression, it is obvious that the output x_i is given the greatest weight when it contains the least noise (i.e., $r_n^{ii} < r_n^{jj}$, $i \neq j$).

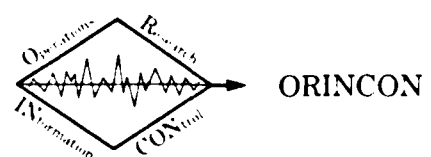
The accuracy of the estimator is dictated, primarily by the number N of sensors. For simplicity suppose that the noise is identically distributed so that

$$r_n^{ii} \triangleq \sigma_n^2 \quad \text{for all } i = 1, 2, \dots, N.$$

Then,

$$\begin{aligned} \sigma_s^2 &= \left[\sum_{i=1}^N 1/\sigma_n^2 \right]^{-1} \\ &= \sigma_n^2/N. \end{aligned} \tag{2.30}$$

The error variance is inversely proportional to the number of sensors. This dependence is valid even when the noise is not identically distributed. Only the constant of proportionality is changed. In fact, R_n does not have to be diagonal for the proportionality of σ_s^2 with $1/N$ to be true.



The observation that the error variance is inversely proportional to the number of sensors reflects the lack of any assumptions regarding the time-variation of the signal $s(t)$. Generally, noise effects are reduced by processing redundant measurements. In the case considered thus far, all redundancy is provided by combining the outputs from the array sensors (i.e., spatial redundancy). Without introducing any structure regarding the time-variation of signal, further error reduction is not possible. We shall return to this aspect later in the discussion.

II.4.2 The Maximum Likelihood Estimator and Adaptive Arrays

The estimator (2.29) can be obtained from other points-of-view that are useful for considering other aspects of the general problem. In particular, it is convenient to assume that the noise is jointly Gaussian with probability density function

$$f_N(\underline{n}'(t)) = (2\pi)^{-N/2} (\det R_{n'})^{-\frac{1}{2}} \exp\left\{-\frac{1}{2} \underline{n}'^T(t) R_{n'}^{-1} \underline{n}'(t)\right\}. \quad (2.31)$$

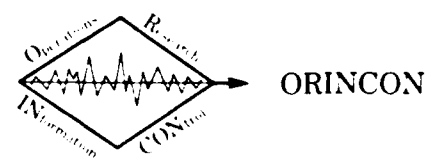
But this can be rewritten in terms of the unknown signal using (2.16). One obtains

$$\begin{aligned} f_N(\underline{n}'(t)) &= (2\pi)^{-N/2} (\det R_{n'})^{-\frac{1}{2}} \exp\left\{-\frac{1}{2} [\underline{x}(t) - \underline{s}(t)]^T R_{n'}^{-1} [\underline{x}(t) - \underline{s}(t)]\right\} . \end{aligned} \quad (2.32)$$

Using (2.32), we can now determine the maximum likelihood estimator of $\underline{s}(t)$. The likelihood equation [11] for $\underline{s}(t)$ is

$$\frac{\partial}{\partial \underline{s}} [\underline{x}(t) - \underline{s}(t)]^T R_{n'}^{-1} [\underline{x}(t) - \underline{s}(t)] = 0.$$

Carrying out the differentiation with respect to \underline{s} , one obtains the equation



$$\underline{1}^T \underline{R}_{n'}^{-1} [\underline{x}(t) - \hat{\underline{s}}_{ML} \underline{1}] = 0.$$

When solved, the maximum likelihood estimator of s is seen to be

$$\begin{aligned}\hat{s}_{ML}(t) &= \frac{\underline{1}^T \underline{R}_{n'}^{-1}}{\underline{1}^T \underline{R}_{n'}^{-1} \underline{1}} \underline{x}(t) \\ &\equiv \hat{s}_{AMS}(t).\end{aligned}\quad (2.33)$$

Thus, under the assumption that the noise is Gaussian, the minimum mean-square and maximum likelihood estimators of $s(t)$ are identical.

In (2.29) and in (2.33), it is assumed that the noise covariance matrix $\underline{R}_{n'}$ is known. For seismic surveillance, it is unrealistic to assume that $\underline{R}_{n'}$ is known for all times. In fact, the noise covariance matrix must be estimated from the sensor outputs. The repeated estimation of $\underline{R}_{n'}$ provides the basis for adaptive array processing.

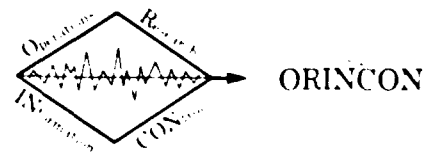
The noise covariance matrix can be estimated from samples of the outputs of the N sensors. In the absence of a signal

$$\underline{x}(t) = \underline{n}'(t).$$

Suppose that the outputs are samples at times $t_k = kT$, $k = 0, 1, \dots, M-1$. Then, the maximum likelihood estimator of the noise covariance matrix is given by

$$\hat{\underline{R}}_{n'} = \frac{1}{M} \sum_{i=0}^{M-1} \underline{x}(iT) \underline{x}^T(iT) \quad (2.34)$$

The accuracy of this estimator depends upon the number of independent samples used to form $\hat{\underline{R}}_{n'}$. The independence of the samples is ensured by the choice of the sampling interval T . As indicated in [11, 12], satisfactory estimates are often obtained



by using twice as many independent samples as there are sensors ($M \geq 2N$).

The estimator $\hat{R}_{n'}$ must be computed in the absence of any signal. In order to adapt to a changing noise environment, the estimator $\hat{R}_{n'}$ must be recomputed. Then, $\hat{R}_{n'}$ must be inverted in order to determine the weighting vector. To simplify the calculations, the inverse $\hat{R}_{n'}^{-1}$ can be computed recursively, thereby permitting a recursive computation of the weighting vector. These recursive relations are obtained using the Sherman-Morrison lemma [11] of matrix algebra which are stated below.

The maximum likelihood estimator, using $\hat{R}_{n'}$, is given by

$$\hat{s}_{ML}(t) = \frac{\underline{1}^T \hat{R}_{n'}^{-1} \underline{1}}{\underline{1}^T \hat{R}_{n'}^{-1} \underline{1}} \underline{x}(t)$$

$$= \frac{\underline{1}^T P}{\underline{1}^T P \underline{1}} \underline{x}(t)$$

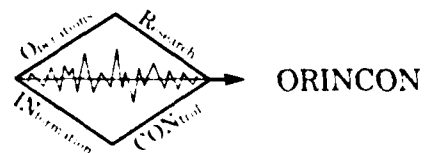
where

$$P \triangleq \left[\sum_{i=0}^{M-1} \underline{x}(iT) \underline{x}^T(iT) \right]^{-1} .$$

Let us denote P explicitly in terms of the number of samples used in its formation.

$$\begin{aligned} P(k+1) &\triangleq \left[\sum_{i=0}^k \underline{x}(iT) \underline{x}^T(iT) \right]^{-1} \\ &= [P^{-1}(k) + \underline{x}(kT) \underline{x}^T(kT)]^{-1} . \end{aligned}$$

Using the Sherman-Morrison lemma [11], this becomes



$$P(k+1) = P(k) - \frac{P(k) \underline{x}(kT) \underline{x}^T(kT) P(k)}{1 + \underline{x}^T(kT) P(k) \underline{x}(kT)} . \quad (2.34)$$

It is important to recognize that no matrix inversion is required after $P(1)$ is formed.

The inverse of the sample covariance matrix is determined, except for the multiplication by the number of samples, by evaluating (2.34). The matrix is caused to adapt to the changing noise environment by continually introducing noise samples, separated sufficiently in time to ensure independence. The adaptation is enhanced by introducing a fading memory into the calculation by redefining $P(k+1)$ as

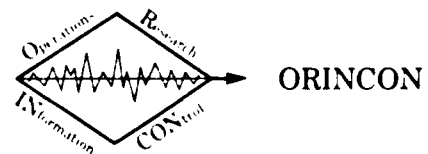
$$P(k+1) = [\alpha(k) P^{-1}(k) + \underline{x}(kT) \underline{x}^T(kT)]^{-1} .$$

The scalar parameter $\alpha(k)$, $0 < \alpha \leq 1$, is the fading factor and causes the past measurements to be given less weight when $\alpha < 1$ than the current measurement. It follows easily, assuming that a fading factor is introduced at every step that $\underline{x}[(k-1)T]$ is faded by $\alpha(k)$, $\underline{x}[(k-2)T]$ is faded by $\alpha(k-1) \alpha(k)$, and in general $\underline{x}[(k-l)T]$ is multiplied by $\alpha(k) \alpha(k-1) \dots \alpha(k-l-1)$. Thus, older samples are given much less weight than the most recent sample. The fading memory maximum likelihood estimator is defined as

$$\hat{s}_{ML}^\alpha(t) = \underline{w}_{ML}^{\alpha T}(k+1) \underline{x}(t) \quad (2.35)$$

where

$$\underline{w}_{ML}^{\alpha}(k+1) \triangleq \frac{P^{\alpha}(k+1) \underline{1}}{\underline{1}^T P^{\alpha}(k+1) \underline{1}} \quad (2.36)$$



and

$$P^\alpha(k+1) = \bar{P}(k) - \frac{\bar{P}(k) \underline{x}(kT) \underline{x}^T(kT) \bar{P}(k)}{1 + \underline{x}^T(kT) \bar{P}(k) \underline{x}(kT)}$$

$$\bar{P}(k) \triangleq \frac{1}{\alpha(k)} P^\alpha(k).$$

With (2.35), a data-directed procedure for determining the array weights has been defined. The signal is estimated using (2.35) and the array pattern that results is obtained by using (2.36) in (2.20). The array sensitivity can be established and signal estimates are computed. It is appropriate now to consider the problem of detecting the presence of a signal in the prescribed beam direction.

II.4.3 The Signal Detection Problem

To provide a basis for signal detection, assume as in (2.31) that the noise is multivariate Gaussian. Then, at each sampling time, the detection problem can be stated in terms of two hypotheses H_0 and H_1 .

H_0 : no signal present

$$\underline{x}(t) = \underline{n}'(t)$$

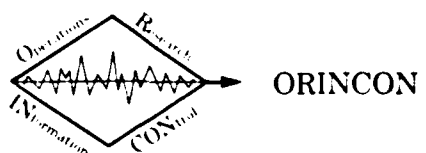
H_1 : signal present

$$\underline{x}(t) = \underline{s}(t) \perp + \underline{n}'(t)$$

where $\underline{n}'(t)$ has the Gaussian distribution given by (2.31). For the moment, it is assumed that the noise covariance $R_{n'}$ is known. Also, the signal is assumed to be unknown but nonrandom.

The likelihood ratio

$$\Lambda \triangleq \frac{f(\underline{x}|H_1)}{f(\underline{x}|H_0)} \quad (2.37)$$



is well-known [e.g., see Reference 13] to provide the optimal detector, for example, for the Neyman-Pearson criterion. In (2.37), $f(\underline{x}|H_i)$ represents the probability density function for the output \underline{x} under the hypotheses H_i , $i = 0, 1$. From the definition, the output \underline{x} is seen to have a Gaussian distribution under both hypotheses. The covariance of \underline{x} is the same for both cases and the distributions differ only because the mean values are different.

$$f(\underline{x}|H_0) = (2\pi)^{-N/2} (\det R_{n'})^{-1/2} \exp \left\{ -\frac{1}{2} \underline{x}^T(t) R_{n'}^{-1} \underline{x}(t) \right\} \quad (2.38a)$$

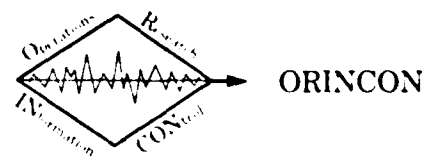
$$\begin{aligned} f(\underline{x}|H_1) = (2\pi)^{-N/2} (\det R_{n'})^{-1/2} \exp & \left\{ -\frac{1}{2} [\underline{x}(t) - \underline{s}(t)]^T \right. \\ & \left. \cdot R_{n'}^{-1} [\underline{x}(t) - \underline{s}(t)] \right\}. \end{aligned} \quad (2.38b)$$

Substituting (2.38) into (2.37) obviously allows the normalizing constant $(2\pi)^{-N/2} (\det R_{n'})^{-1/2}$ to be ignored. To eliminate the exponential, the logarithm can be taken without changing the nature of the hypothesis test. Then, one obtains after straightforward manipulations, the following test.

$$\begin{matrix} H_1 \\ s(t) \underline{1}^T R_{n'}^{-1} \underline{x}(t) > \lambda \\ H_0 \end{matrix} \quad (2.39)$$

where the choice of λ is based upon the desired false alarm and detection probabilities. Equation (2.39) indicates that the output $\underline{x}(t)$ is correlated with the signal $\underline{1}s(t)$ after normalizing with the inverse of the noise covariance matrix $R_{n'}^{-1}$.

There is a major problem that arises in the application of (2.39) to the seismic signal processing problem. Neither the noise covariance matrix $R_{n'}$ nor the signal is known. As discussed above, the noise covariance $R_{n'}$ can be estimated using the sample covariance matrix obtained from output samples obtained in the absence of any signal. Next, the signal $s(t)$ can be estimated using (2.35). The generalized likelihood ratio test proceeds by replacing the unknown parameters in



the likelihood ratio test by the best estimates of the parameters. In this case, (2.39) is rewritten as

$$\hat{s}_{ML}(t) \underline{1}^T \hat{R}_n^{-1} \underline{x}(t) \begin{matrix} > \\ < \end{matrix}_{H_0}^{H_1} \lambda$$

or

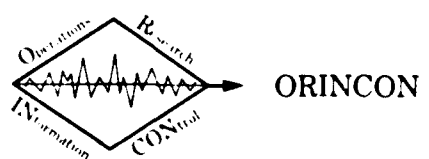
$$\hat{s}_{ML}(t) \underline{1}^T P \underline{x}(t) \begin{matrix} > \\ < \end{matrix}_{H_0}^{H_1} \frac{\lambda}{M}. \quad (2.40a)$$

But this further reduces to

$$\frac{[\underline{1}^T P \underline{x}(t)]^2}{\underline{1}^T P \underline{1}} \begin{matrix} > \\ < \end{matrix}_{H_0}^{H_1} \frac{\lambda}{M}. \quad (2.40b)$$

Thus, one can use the left-hand side of either (2.40a) or (2.40b) to define the test statistic for the hypothesis test.

In (2.40b), a quadratic form is determined as the test statistic. This quadratic form could be recognized as a χ^2 -variable with a single degree of freedom were P to be a deterministic or known matrix rather than a random variable formed from the sample covariance matrix. If P were known, the hypothesis test could be evaluated using the χ^2 -distribution to evaluate the probability of detection and probability of false alarm for a prescribed threshold value λ . By ignoring the random character of P , approximate probabilities of detection and false alarm could be determined [13].



II. 4. 4 The Effect of Signal Models

In the previous discussion, no assumptions were made regarding the character of the signal. As a result, the signal estimator in (2.35) is based entirely on the aligned outputs of the N sensors. Further understanding of the estimation problem is obtained by introducing assumptions regarding the signal and reconsidering the preceding analysis. As discussed above, a seismic surveillance system may be required to detect either narrowband or wide band signals, depending upon the nature of the target. Both types of signals shall be considered below and related to the preceding results.

Narrowband Signals: Suppose that the signal energy is known to be concentrated at some center frequency ω_c . It has been proven [e.g., see References 8, 12 or 14] that for narrowband signals, the structure of the optimal estimator is given by

$$\hat{s}(t) = \underline{w}^T \underline{x}(t)$$

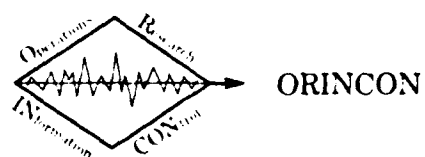
where

$$\underline{w} = \beta R_n^{-1} \underline{1}.$$

The parameter β is a scalar that follows from the optimality criterion (e.g., minimum variance, minimum mean-square error, maximum signal-to-noise ratio). Thus, the results obtained above are not changed significantly when attempting to detect the existence of a narrowband signal.

The relationship between estimators can be defined more precisely and their examination provides insight into the interrelations. Suppose that S represents the signal power in the narrowband signal. The noise power is defined from the earlier discussion to be

$$N_0 = \underline{1}^T R_n^{-1} \underline{1}.$$



Then, the weight vector that results in the largest output signal-to-noise ratio is given by

$$\underline{w}_{SNR} = \underline{R}_{n'}^{-1} \underline{1}. \quad (2.41a)$$

The weight vector for the maximum likelihood estimator is given by

$$\underline{w}_{ML} \triangleq \frac{1}{N_0} \underline{w}_{SNR}. \quad (2.41b)$$

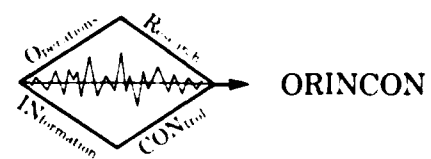
Assuming that the signal is narrowband with power S, the mean-square error is minimized with the weight vector

$$\underline{w}_{MSE} = \frac{SN_0^2}{SN_0^2 + N_0} \underline{w}_{ML}. \quad (2.41c)$$

As discussed earlier, the structure of the estimator is provided essentially by forming the gain (2.41a). Estimators for other optimality criteria are obtained by simple scalar operations.

It is interesting to note that the center frequency of the narrowband signal does not appear explicitly in the estimator. To implement the MMSE estimator, the signal power S must be known. In many cases, the maximum likelihood estimator (2.41b) appears to provide the most satisfying approach.

Broadband Signals: We have seen that the estimation error is proportional to the number of sensors. To reduce the errors for a fixed number of sensors having a prescribed geometry, one must consider the temporal behavior of the signal. For a band limited signal with maximum frequency of f_m Hz, it is well known that the signal can be reconstructed from uniformly-spaced samples obtained at a rate of $2f_m$ samples/second. Based on this realization, the estimation of the signal $s(t)$ can be formulated in terms of an appropriate number of delayed samples of the output of each sensor in addition to the signal-aligned samples. Essentially, the sensor outputs are filtered before summing and estimating.



Weighted tap-delay lines can be introduced to accomplish optimal signal estimation for broadband signals [15]. The development of the approach reduces to the previous discussion through the appropriate redefinition of the relevant quantities. This occurs at the expense of a greatly increased dimensionality of the matrices and vectors that are treated. We shall demonstrate the reformulation of the problem in the subsequent paragraphs.

Suppose that L uniformly-spaced samples of each sensor output are to be utilized to estimate the broadband signal $s(t)$. The sampling interval is chosen consistent with the highest frequency component of the signal. The outputs of each delay are multiplied by weights w_i which are chosen to obtain a suitable estimator of the signal. Notationally, let

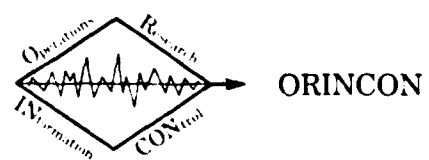
$$\begin{aligned}\underline{x}_1^T &\triangleq [x_1(t), x_2(t), \dots, x_N(t)] \\ \underline{x}_2^T &\triangleq [x_1(t-\Delta), x_2(t-\Delta), \dots, x_N(t-\Delta)] \\ &\vdots \\ \underline{x}_L^T &\triangleq [x_1[t-(L-1)\Delta], x_2[t-(L-1)\Delta], \dots, x_N[t-(L-1)\Delta]]\end{aligned}$$

and

$$\underline{x}^T \triangleq [\underline{x}_1^T, \underline{x}_2^T, \dots, \underline{x}_L^T].$$

Similarly, let

$$\begin{aligned}\underline{w}_i^T &\triangleq [w_{1i}, w_{2i}, \dots, w_{Ni}], \quad i = 1, 2, \dots, L \\ \underline{w}^T &\triangleq [\underline{w}_1^T, \underline{w}_2^T, \dots, \underline{w}_L^T]\end{aligned}$$



and

$$\hat{s}(t) = \sum_{i=1}^L \underline{w}_i^T \underline{x}_i \triangleq \underline{w}^T \underline{x} . \quad (2.42)$$

It is apparent that the signal estimator (2.42) has the same form as introduced in (2.15) at the beginning of this discussion. The dimension associated with the weight vector \underline{w} is now equal to LN rather than N. Thus, the earlier developments and remarks can be applied, virtually without modification except for matters dealing with dimensionality. For example, the noise covariance matrix R_n' is, now, an $(LN \times LN)$ matrix. Since it must be inverted to determine the optimal gains, one can be faced with a substantial computational burden. However, the uniformity of the delays causes the matrix R_n' to be block Toeplitz. Consequently, there exist efficient numerical algorithms that can be used to determine $R_n'^{-1}$.

The Toeplitz structure of the noise covariance matrix is demonstrated easily. Suppose that \underline{n}_k represents the noise in the output \underline{x}_k , noting that

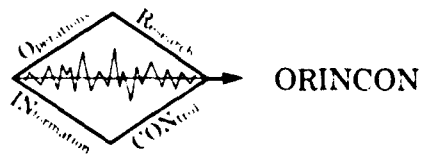
$$\underline{n}_k^T = [n_1[t-(k-1)\Delta], n_2[t-(k-1)\Delta], \dots, n_N[t-(k-1)\Delta]] .$$

Then, it is apparent that

$$\begin{aligned} E[\underline{n}_k \underline{n}_{k+\ell}^T] &= \{r^{ij}(\ell\Delta)\} \\ &= R_\ell \end{aligned}$$

where

$$\begin{aligned} r^{ij}(\ell\Delta) &= E \left\{ n_i[t-(k-1)\Delta] n_j[t-(k+\ell-1)\Delta] \right\} \\ &= E[n_i(k\Delta) n_j(k+\ell)\Delta] . \end{aligned}$$

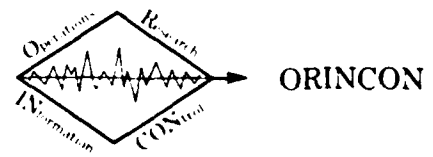


The covariance matrix depends only on the delay difference and it follows that it has the following structure.

$$R_n = E[\underline{n}\underline{n}^T] = \begin{bmatrix} R_0 & R_1 & \cdots & R_{L-1} \\ R_{-1} & R_0 & \cdots & R_{L-2} \\ \vdots & \ddots & \ddots & \vdots \\ R_{1-L} & R_{2-L} & \cdots & R_0 \end{bmatrix}. \quad (2.43)$$

But this is a block Toeplitz matrix as was asserted above.

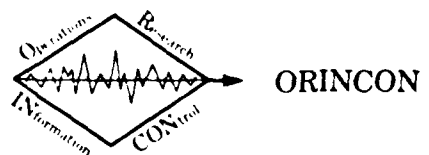
Because of the block Toeplitz form of the noise covariance matrix, computationally-efficient algorithms exist for finding the inverse R_n^{-1} or for the solution of the normal equations to determine the optimal gains. For example, the Toeplitz matrix inversion algorithm of Trench [6] could be used. Alternatively, the multivariable form of the Levinson algorithm could be utilized to determine the weight vector [17].



PART III
GENERAL ALGORITHMS AND RECOMMENDATIONS

ABSTRACT

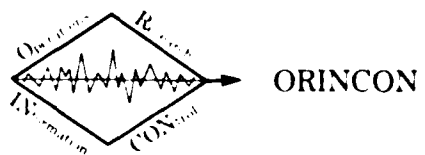
The conclusions and major results of Parts I and II are summarized in the following pages. The theme of this presentation has been to identify important physical characteristics of the signals generated by a seismic source. These characteristics have been used to define general signal processing algorithms that can provide an appropriate framework for the design and analysis of specific algorithms. Because of the intrinsic complexity of the operational environment and of the limitations on the deployed system, it is imperative that the greatest processing gain possible is achieved. The general approach that is presented in Part III should provide a performance baseline for evaluating any processor. Furthermore, it permits great flexibility in the design of signal processors for the operational system.



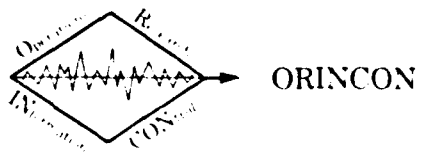
III.1 General Algorithmic Considerations

In this section, the lengthy discussions that have appeared above are summarized by identifying the fundamental computations that must be accomplished. First, some general observations are required.

1. An essential aspect of the detection/estimation problem that has been defined appears in the estimation of the noise covariance matrix R_n (or, equivalently, its inverse). The estimated covariance matrix \hat{R}_n must be repeatedly determined from sensor outputs. The reestimation of R_n provides the adaptive capability of the array processor. This can be accomplished in a variety of ways. For example [8], the Widrow's LMS filter or the Howells-Applebaum adaptive processor are based, essentially, on the covariance estimation. As discussed by Reed, et. al. [12], more rapid convergence is achieved by working directly with the covariance matrix and its inverse. This increased convergence is achieved at the cost of a greater computational burden. We propose the direct approach here for two major reasons.
 - (i) It is desirable at this early stage of the development of a seismic surveillance system to obtain some idea of the best convergence that can be achieved. Also,
 - (ii) It is likely that the arrays used in an operational seismic surveillance system may not use an excessively large number of sensors. Then, the computational burden might not be excessive. Furthermore, with a limited number of sensors, rapid convergence becomes particularly important.



2. In order to ensure that \hat{R}_n adapts to changing noise conditions, it is necessary that new samples of the sensor outputs be given greater emphasis than outdated samples. While this effect can be assured by defining a fixed "window" of samples in computing \hat{R}_n , finite-memory filters generally are computationally burdensome and require considerable amount of storage. Thus, a recursive updating procedure that incorporates a fading memory may offer a significant advantage. Although not discussed here, many nonrecursive methods can be used to obtain \hat{R}_n , including the FFT and spectral estimation.
3. The computation and display of the magnitude of the array pattern can provide geometric insights into the response of the processor for arbitrary array configurations and geometries. As discussed, the generalized array pattern incorporates the weighting vector of the signal estimator. Although discussed only in passing, the array pattern can be modified to incorporate any directional limitations of the sensor. For example, a vertical seismometer is not sensitive to a direct P-wave. The array processor and its attendant pattern should incorporate this information in testing for each type of seismic wave.
4. Throughout this discussion, restrictive assumptions regarding the signal structure have been carefully avoided. In Section II.4.4, the development was seen to apply directly to narrowband signals. However, at the cost of increased dimensionality, the results were extended to broadband signals through the use of tapped-delay lines and some subsequent notational changes. Reasonable assumptions could be introduced that would reduce the dimension of the filter development for broadband signals. At this early stage of development, more involved models seem inappropriate. However, separate processors for narrowband and for broadband signals appear to be desirable.



AD-A102 993

ORINCON CORP LA JOLLA CA
SIGNAL PROCESSING FOR SEISMIC SURVEILLANCE.(U)
JUL 81 H W SORENSEN
OC-R-81-3090-2

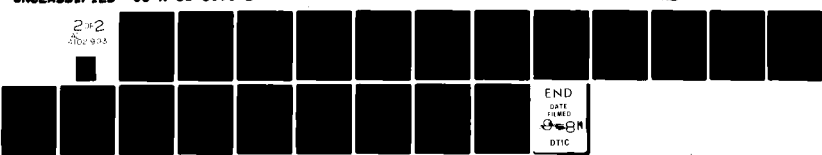
F/6 8/11

N00014-79-C-0390

NL

UNCLASSIFIED

242
242-93

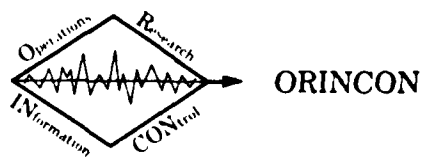


END
DATE
FILED
OCT 11 1981
DTIC

5. In the formulation of the problem, it is not difficult conceptually to place pattern nulls in the direction of known interference sources. The computational burden is increased, however, and one must expect the convergence rate of the processor to be affected. In the following, we shall not explicitly describe the inclusion of pattern nulls, although this subject has been discussed in Part II.
6. There are many questions regarding parameter choices and processor performance that can be resolved primarily through numerical experimentation using both simulated and real data. In fact, simulations based on reasonable models of the sensor outputs should be used for all preliminary testing and for development of the algorithms.
7. As discussed in Part I and Section II.1.1, the components (i.e., the outputs of the horizontal and the vertical seismometers) of the 3-axis geophones can be used to classify the type of seismic wave that is detected. By defining classification procedures that are based on the physical properties of the wave propagation, the range of speeds and directions that must be considered can be limited appropriately to reduce the computational burden.
8. The propagation of seismic energy from the source to an array of sensors has a very complex description. Several propagation paths are possible; the effect of the earth upon a specific propagation path is itself very difficult to describe or predict. Consequently, it is generally unrealistic to introduce detailed mathematical models of the signal for the definition of the processing algorithms. For this presentation, the primary assumptions are the following.

- (i) The elements of a single array are spaced sufficiently close that the passing wave can be regarded as having a planar wave front with a direction β and average speed c .
- (ii) The signal sensed by similar elements (e.g., the vertical seismometer) of the array is identical except for a time shift that depends upon the array geometry and the wave front properties.
- (iii) Signals are band limited and can be either narrowband or broadband. Other than this qualitative description of the signal, mathematical models are not defined for the model.

The processing gain of the array for narrowband signals is provided primarily by the number of sensors in the array. For broadband signals, tapped delay lines can be used to incorporate the redundancy provided by successive samples of the sensor outputs. As discussed in Section II.4, the Toeplitz form that obtains using tapped delay lines permits the development of efficient computational algorithms for inverting R_n .



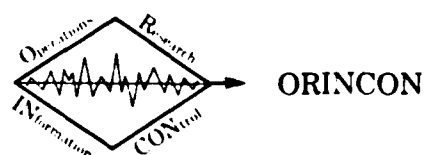
III.2 Structure of the General Algorithms

A seismic signal processor must provide the following capabilities.

1. Detection: The existence of a signal must be detected from the sensor outputs. The performance of the detector must be assessed, typically by determining the Receiver Operating Curve (ROC) (i.e., the probability of detection versus the probability of false alarm).
2. Estimation: The direction β and the speed c of the detected wave front must be estimated. The quality of the estimates in terms of bias and error variance must also be determined. In addition, signal characteristics must be estimated. For example, an estimate of the center frequency of a narrowband signal should be determined. For a broadband signal, the time-of-arrival of the signal may be a desirable parameter to know. Also, the bandwidth of the signal should be estimated.

In order to discriminate between signals and noise, it is imperative that the noise covariance matrix is estimated. These estimates must be updated continually from samples that are obtained in the absence of the signal. As discussed in Part II and summarized below, the noise covariance matrix (or its inverse) provides the basis for any signal processing algorithm.

3. Classification: From estimates relating to the detected signals, it is necessary that the type of signal source is determined. The features of the signal have been discussed in Part I and these characteristics should provide the basis for a classification procedure. The performance of a classifier will depend upon the quality of the detection/estimation algorithms so will not be addressed herein. It should be noted that the source of narrowband energy will often be moving (e.g., a truck, tank, or aircraft). The motion of the source will introduce



an additional property to the sensor outputs that may assist in the classification problem.

The approach that has been discussed in Part II and which is summarized below is based upon the continuing estimation of the noise covariance matrix. The estimation must be accomplished for time-lagged versions of the noise-only sensor outputs that are consistent with the range of delays implied by the signal directions and speeds that are to be considered. The covariance matrix is used in a processor that is formed as a concatenation of a beamformer and a detector. The beamformer produces estimates of the signal parameters that are used in a generalized maximum likelihood detector. Source classification can be accomplished following the detection. Let us now review the basic ingredients of the proposed signal processor.

Array Outputs

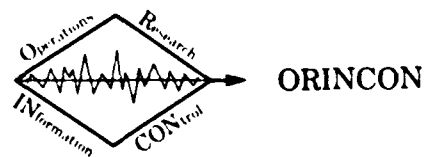
$$z_i(t), \quad i = 1, 2, \dots, N.$$

The sensor output records must be sampled at a rate consistent with highest frequency in an anticipated signal. The sampling rate also must be chosen to be compatible with the delays introduced in the beamforming operation and in the tapped-delay lines used for broadband signals. Because of the use of sampled-data, beamforming is accomplished for a finite number of beam angles.

Signal Alignment (Beamforming)

The signals are aligned by delaying the outputs of sensors at location r_i by the amount

$$\hat{\tau}_i = -\frac{\hat{s} r_i}{c}.$$



The beam direction is $\hat{\beta}$ and \hat{c} represents an estimate of the wave speed. For a fixed $\hat{\beta}$, several estimates of \hat{c} are introduced whose value depends upon the type of seismic wave that is sought. The best estimate of the speed \hat{c} is based upon the detector output (as discussed below). The signal-aligned outputs are denoted as

$$\underline{x}_i(t), \quad i = 1, 2, \dots, N$$

and, implicitly, depend upon $\hat{\beta}$ and \hat{c} . For convenience, we shall denote

$$\underline{x}^T(t) \triangleq [x_1(t), x_2(t), \dots, x_N(t)].$$

Covariance Estimation

It was shown in Section II.4 that optimal signal estimators having the general form

$$\hat{s}(t) = \underline{w}^T \underline{x}(t)$$

are characterized such that

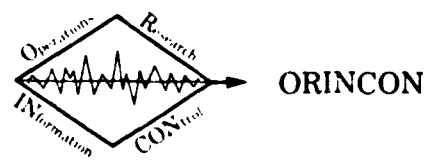
$$\underline{w} = \gamma R_n^{-1} \underline{1}$$

where

$$\underline{1}^T \triangleq (1, 1, \dots, 1).$$

Different estimation criteria produce specific values for γ . Consequently the inverse of the noise covariance matrix provides the fundamental information required to estimate $s(t)$. Note that it is the inverse, not R_n , that is required.

For seismic surveillance, it is unreasonable to expect that R_n^{-1} is known a priori. In fact, it is not even realistic to assume that the covariance matrix is constant during a long period of time. Thus, an adaptive processor will estimate R_n and use the estimate \hat{R}_n to determine the weighting vector for the array processor. Because it is desirable



to ensure that this estimate is most sensitive to the current data, it seems reasonable to determine \hat{R}_n recursively. That is, new output data is incorporated into the estimator as a direct update of the last estimate. To reduce the influence of data that may have been obtained at a time more distant than is consistent with the stationarity assumption, a fading factor α can be introduced.

Let P denote a matrix that is proportional to \hat{R}_n^{-1} . Then, P can be updated recursively according to

$$P(k) = \frac{1}{\alpha(k)} P^\alpha(k), \quad 0 < \alpha(k) \leq 1$$

where

$$P^\alpha(k+1) = P(k) - \frac{P(k) \underline{x}(kT) \underline{x}^T(kT) P(k)}{1 + \underline{x}^T(kT) P(k) \underline{x}(kT)}.$$

The vector $\underline{x}(kT)$ represents the output sample that is used to obtain the new estimate of \hat{R}_n (or \hat{R}_n^{-1}). Note that the covariance estimate is obtained from samples for which it is assumed that no signal is present. Furthermore, samples used to estimate R_n must be obtained at times that are separated sufficiently that the samples can be regarded as being statistically independent.

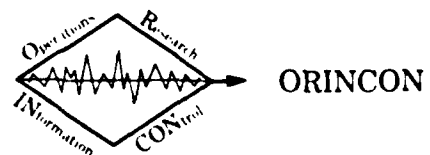
Signal Estimation

Using P , the maximum likelihood estimator of the signal is given by

$$\hat{s}_{ML}(t) = \underline{w}_{ML}^T(k+1) \underline{x}(t)$$

where

$$\underline{w}_{ML}(k+1) \triangleq \frac{1}{\underline{1}^T P^\alpha(k+1) \underline{1}} P^\alpha(k+1) \underline{1}.$$



Signal Detection

The presence of a signal is denoted by hypothesis H_1 whereas its absence is the hypothesis H_0 . The generalized likelihood ratio test requires the correlation of the sensor output with $\hat{s}_{ML}(t)$. The test can be written as

$$\frac{\hat{s}_{ML}(t) \underline{1}^T P^\alpha(k+1) \underline{x}(t)}{\underline{1}^T P^\alpha(k+1) \underline{1}} \stackrel{H_1}{>} \lambda_M \stackrel{H_0}{<}$$

or, equivalently, as

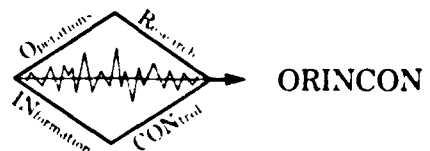
$$\frac{[\underline{1}^T P^\alpha(k+1) \underline{x}(t)]^2}{\underline{1}^T P^\alpha(k+1) \underline{1}} \stackrel{H_1}{>} \lambda_M \stackrel{H_0}{<}.$$

When the LHS of the inequality exceeds the threshold λ_M , the signal is said to be present. Otherwise, the output is regarded as noise only.

Note that the signal estimate does not actually have to be computed to perform the signal detection test. Again, this emphasizes the central role that must be played in the processor by the inverse of the noise covariance matrix P .

The performance of the detection test is dictated by the choice of the threshold parameter λ_M . A precise analysis of the detector is difficult since P^α is a random quantity. However, estimates of the probability of detection and false alarm, and, subsequently, the generation of receiver operating curves (ROC) can be accomplished with the introduction of the following assumptions:

1. Suppose that P^α is not a random quantity. That is, treat this matrix as the true and known value of R_n^{-1} .
2. Assume that \underline{x} is Gaussian. Then, the LHS of the inequality can be regarded as a χ^2 -variable. We shall not pursue the analysis of the detector at this time. The general results of Reference [13] provide additional details.



Array Pattern

A basic tool for the analysis of an array configuration and signal estimator is provided by examining the array pattern $A(\omega, \underline{v}, \underline{w})$ where

$$A(\omega, \underline{v}, \underline{w}) = \sum_{i=1}^N w_i e^{-j\omega v^T \underline{r}_i}$$

and

$$\underline{v} \triangleq \left(\frac{\underline{\beta}}{c} - \frac{\hat{\underline{\beta}}}{\hat{c}} \right)$$

$$\underline{\beta} = \begin{pmatrix} \cos \theta & \sin \phi \\ \sin \theta & \sin \phi \\ \cos \phi \end{pmatrix}$$

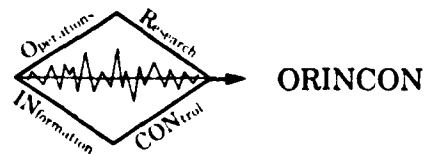
$$\underline{r}_i = r_i \begin{pmatrix} \cos \theta_i \\ \sin \theta_i \\ 0 \end{pmatrix}.$$

Because of the importance of this concept to the evaluation and analysis of a specific array configuration, we shall discuss it in considerable detail.

The analysis is facilitated by considering the variables

$$\eta_x \triangleq \omega \left(\frac{\underline{\beta}_x}{c} - \frac{\hat{\underline{\beta}}_x}{\hat{c}} \right)$$

$$\eta_y \triangleq \omega \left(\frac{\underline{\beta}_y}{c} - \frac{\hat{\underline{\beta}}_y}{\hat{c}} \right).$$



Then, one can write

$$A(n_x, n_y) = \sum_{i=1}^N w_i e^{-j[n_x n_y]} \begin{bmatrix} r_i \cos \theta_i \\ r_i \sin \theta_i \end{bmatrix}.$$

The magnitude $|A(n_x, n_y)|$ can be evaluated as a function of (n_x, n_y) to obtain insights regarding the response for a prescribed array configuration $\{(r_i, \theta_i); i = 1, 2, \dots, N\}$ and prescribed sensor weights $\{w_i; i = 1, 2, \dots, N\}$. The array pattern magnitudes for a linear and for a circular array are shown in Figures III-1 and III-2, respectively.

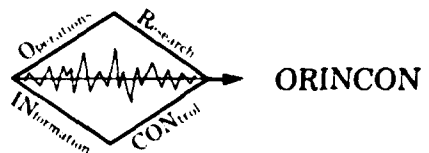
Linear Array

Suppose there are 7 (i.e., $N = 7$) sensors oriented at a 45° angle (i.e., $\theta_i = 45^\circ$ for all i) from the x-axis and located at the points $\{(i, i), i = 1, 2, \dots, 7\}$. Consider equally-weighted sensors with unity weights (i.e., $w_i = 1$) chosen for convenience. In this case, we know that the magnitude of the main lobe equals the number of sensors. Furthermore, it is clear that the magnitude is periodic with period 2π .

In Figure III-1, a printer plot of the magnitude of the array pattern is shown. Lines of equal magnitude are indicated by the digits 0 through 4. The identification is the following.

Plot Character	0	1	2	3	4
Array Magnitude	0.1	2	4	6	7

The plot shows the main lobe and the vestiges of two grating lobes. Clearly, the magnitude is less than 2 for most values of (n_x, n_y) . All of the nulls are not shown because of the scales that have been used. This is easily remedied by appropriate scaling changes. Note also that the directivity of the linear array is suggested by the linear character of the iso-magnitude curves. We shall return to this point, subsequently.



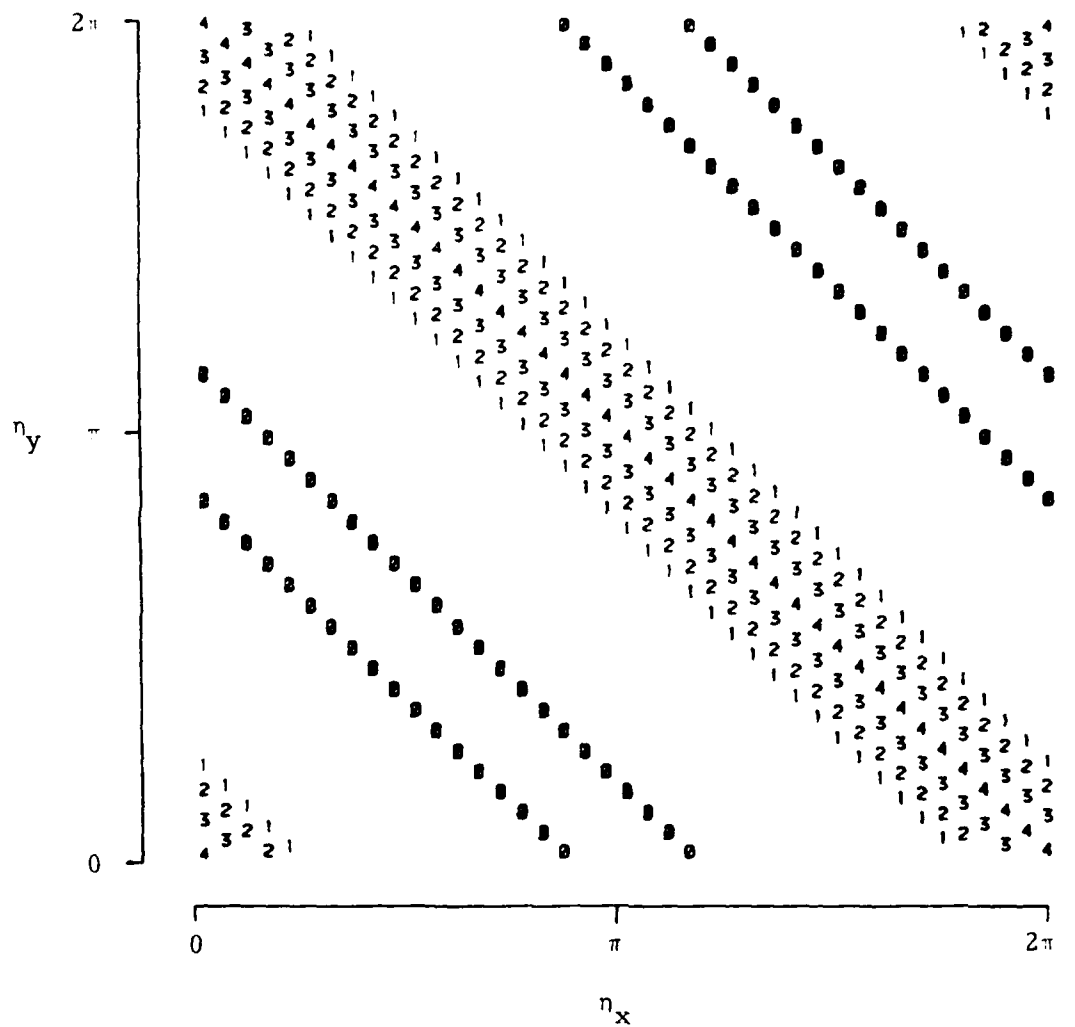


Figure III-1. $A(\eta_x, \eta_y)$ for a linear array.
 $N = 7; w_i = 1, i = 1, 2, \dots, 7.$

Circular Array:

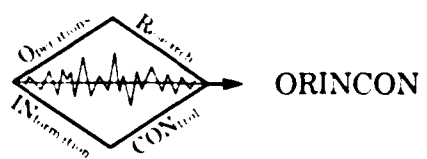
Suppose that 10 (i.e., $N = 10$) sensors are located on a circle of radius 10 (i.e., $r_i = 10$) at equally spaced angles of 36° (i.e., $\theta_{i+1} - \theta_i = 36^\circ$). Assume unity weights (i.e., $w_i = 1$) for all sensors. Therefore, we know that the magnitude of the main lobe is 10.

In Figure III-2, a printer plot of the magnitude of the array pattern is shown. The pattern is much more complicated as indicated by the iso-magnitude lines for the portion of the array pattern that is shown. As indicated, there is a symmetry along radial lines separated by 36° . The plot characters and array magnitudes have the following correspondence.

Plot Character	0	1	2	3	4	5
Array Magnitude	0.2	2	4	6	8	10

The plot indicates the location of the main lobe at $(0,0)$ with secondary lobes scattered about the (η_x, η_y) plane. Nulls can be located from the plot. The range of the plotted variables can be extended further to locate the grating lobes and to further establish the response of the array.

The variables (η_x, η_y) are related to the physical variables $(\omega, c, \beta_x, \beta_y)$ of the problem in a straightforward manner. It is necessary to invert the relationship given above in order to obtain greater physical appreciation for the plots that have been presented. It is reasonable to consider fixed values of frequency ω and wave speed c for a beam direction $\hat{\beta}$. In particular, assume that $c = \hat{c}$ and suppose that the narrowband signal has center frequency ω_c . Then, it is easy to establish a graphically simple relationship between (η_x, η_y) and the azimuth and elevation angles (θ, ϕ) of the interference wave.



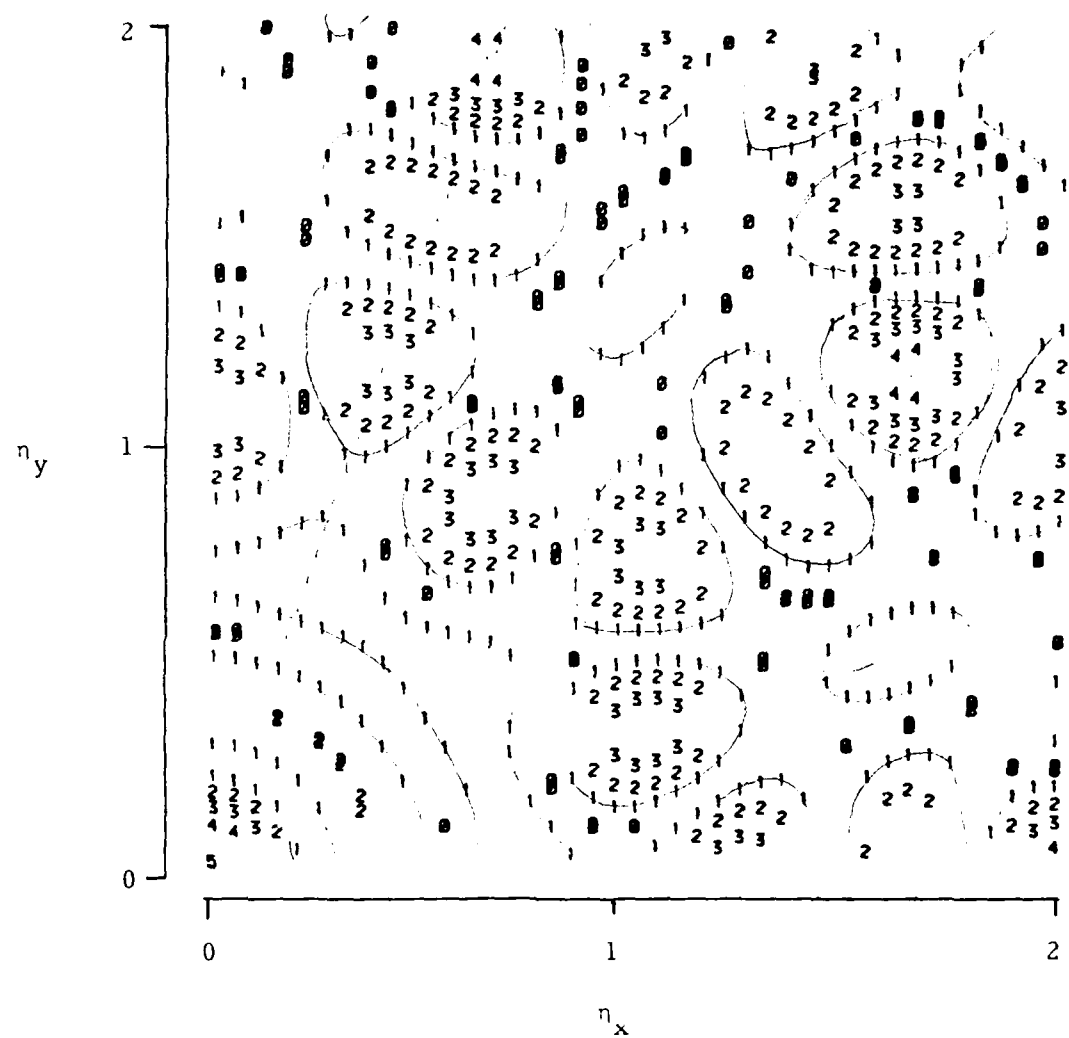
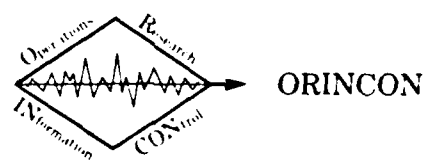


Figure III-2. $A(n_x, n_y)$ for a circular array.

$N = 7; w_i = 1, i = 1, 2, \dots, 10.$



Consider constant values of θ and ϕ , say θ_0 and ϕ_0 , as functions of (n_x, n_y) . Noting that

$$\tan \theta = \frac{\hat{\beta}_y}{\hat{\beta}_x}$$

$$\sin \phi = \pm \sqrt{\hat{\beta}_x^2 + \hat{\beta}_y^2}$$

it is easy to determine for fixed θ_0 that

$$n_y = (\tan \theta_0) n_x + \frac{\omega_c}{c} (\hat{\beta}_x \tan \theta_0 - \hat{\beta}_y).$$

Thus, a constant value of θ induces a linear relationship between n_x and n_y . In fact, it follows that all values of θ have a common point

$$n_x^0 = - \frac{\omega_c}{c} \hat{\beta}_x, \quad n_y^0 = - \frac{\omega_c}{c} \hat{\beta}_y.$$

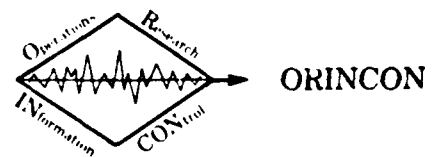
For fixed values ϕ_0 , one finds that

$$\left(\frac{\omega_c}{c} \sin \phi_0 \right)^2 = \left(n_x + \frac{\omega_c}{c} \hat{\beta}_x \right)^2 + \left(n_y + \frac{\omega_c}{c} \hat{\beta}_y \right)^2.$$

Thus, the lines of constant ϕ_0 are given as circles in the (n_x, n_y) plane. The circles are centered at

$$n_x^0 = - \frac{\omega_c}{c} \hat{\beta}_x, \quad n_y^0 = - \frac{\omega_c}{c} \hat{\beta}_y$$

and have radius $|(\omega_c/c) \sin \phi_0|$. Since $|\sin \phi_0| \leq 1$, we see that



$$-\frac{\omega}{c}(\hat{1} + \hat{\beta}_x) \leq n_x \leq \frac{\omega}{c}(\hat{1} - \hat{\beta}_x)$$

$$-\frac{\omega}{c}(\hat{1} + \hat{\beta}_y) \leq n_y \leq \frac{\omega}{c}(\hat{1} - \hat{\beta}_y).$$

The relationship between (n_x, n_y) and (θ, ϕ) is displayed in the following diagram.

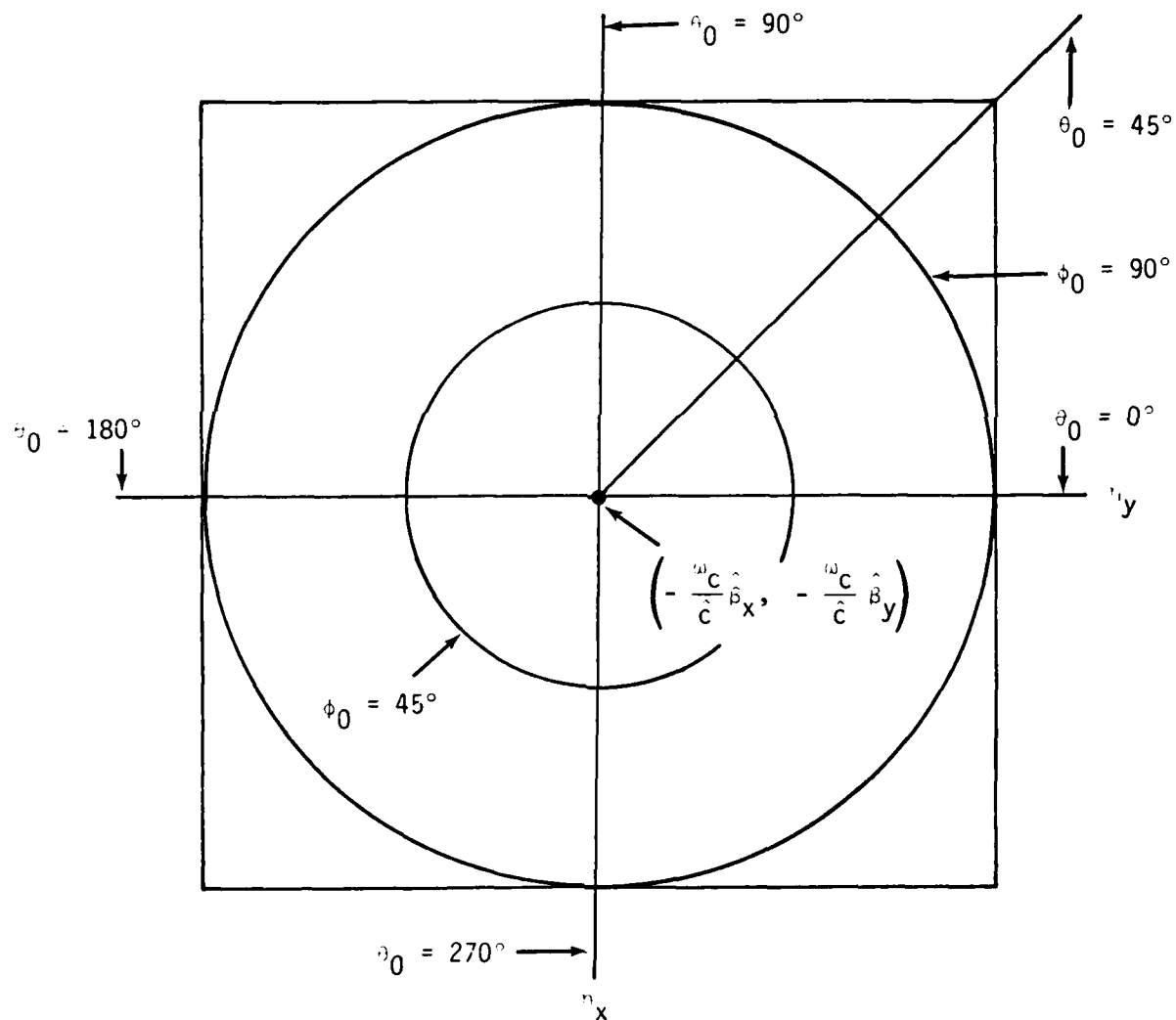
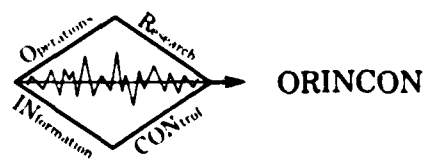


Figure III-3. Azimuth and elevation angles for interference wave.



Note that the origin of the display depends upon the beam direction as defined by $(\hat{\beta}_x, \hat{\beta}_y)$. The frequency ω_c and wave speed c affect the origin and the radius of the circles of constant elevation angles ϕ_0 . Except for the origin, the radial lines that define constant azimuth angles are unaffected by signal characteristics.

The circle of largest radius (i.e., $\phi_0 = 90^\circ$) relates to a horizontal wave. The combination of the radius of this circle, as defined by ω_c/c (i.e., essentially the wave length) with the array pattern dimensions provides a graphical means of determining the sensor spacings that are required to avoid grating lobes.

Note that the main lobe is always located at the point $n_x = 0$, $n_y = 0$. The origin in Figure III-3 is generally nonzero since the main lobe occurs at $\theta_0 = \hat{\theta}$, $\phi_0 = \hat{\phi}$. Thus, the offset of the origin is necessary to ensure that the array is maximally responsive in the direction of the beam.

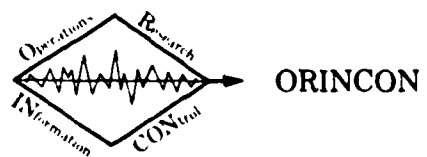
Let us illustrate the use of the array pattern magnitude plot and the transformation from (n_x, n_y) to (θ, ϕ) by considering the linear array whose magnitude is presented in Figure III-1. Attention shall be restricted to horizontal waves (i.e., $\hat{\phi} = 90^\circ = \phi_0$). First, consider a broadside beam (i.e., $\hat{\theta} = 135^\circ$ or $\hat{\theta} = 325^\circ$). Then, the center of the circle in Figure III-3 is given by $(\sqrt{2}\omega_c/2c)(1, -1)$. It is apparent that the circle will be centered along the main lobe ridge emanating from the origin. The radius of the circle is ω_c/c . If $\omega_c/c = \sqrt{2}\pi$, then the array pattern must include the grating lobe. This is seen by superimposing the plot of Figure III-3, suitable scaled, upon Figure III-1. Since the sensors have been assumed to be separated by a distance $\sqrt{2}/2$, we corroborate the assertion in Section II.2 that the spacing of sensors must be greater than $\lambda/2$ to avoid spatial aliasing.

The argument can be repeated for any beam direction and wave characteristics. In fact, the analysis of the aliasing properties of any specific array can be accomplished by superimposing the content of Figure III-3 with suitable scalings on the plot of $|A(n_x, n_y)|$. Although we have not pursued it in the examples, the array pattern can include any weighting values. Consequently, the array response can be examined in detail by using the graphical tools that have been introduced. An interactive graphical display can be developed that can provide the basis for a rapid analysis and evaluation of the array performance.

Wave and Source Classification

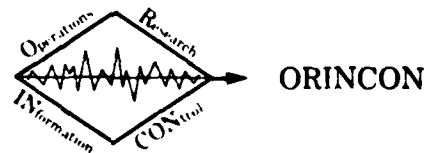
As discussed in Part I, a source can generate several types of seismic waves which can travel along a variety of propagation paths. The output of the signal detector/estimator can be validated by comparing the response of the sets of comparable seismometers to classify the wave type. There must be a consistency in the characteristic of the detected wave (i.e., bandwidths, particle motions, wave speeds, arrival directions) to accomplish a realistic classification. Special purpose algorithms based on the wave characteristics discussed in Part I and in Section II.1 can be defined to accomplish the classification.

A basic objective of the seismic surveillance system is to establish the nature of the source of the detected energy and to locate and, possibly, track potential threats. From the outputs of a single array, it should be possible to distinguish between broadband and narrowband sources. As has been discussed, the direction of the passing wave front shall be estimated and the estimate can be expected to provide some direction-finding capability. However, the complexity of the propagation path may greatly affect the direction of travel of a wave front as it passes from source to array.



Multiple Arrays

To accomplish source localization and tracking, the output from a single array must be combined with other information. The most reasonable source of additional data is another array (or several arrays). We have not discussed interarray processing in this report as it was considered to be beyond the scope of the effort. The processing of data from multiple arrays must be considered as an integral part of the seismic surveillance system.

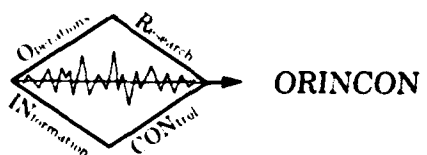


III.3 Recommendations and Summary

This report reflects the basic recommendation of the effort. For the development of a useful seismic surveillance system, it is imperative that the signal processor be developed from a general perspective based upon an understanding of the physical problem. To produce an operational system that provides for the detection of target sources in a timely manner, the signal processor must be able to extract maximal information from the available data. Furthermore, it must be sufficiently flexible that nonstandard conditions and unusual array configurations can be accommodated without serious deterioration in the quality of the processor output. Untimely haste in the implementation of specific algorithms that are inflexible or ill-suited to the physical problem can only be counterproductive.

To establish the performance potential of a seismic surveillance system, it is recommended that the algorithms stated in Section III.2 and discussed in Part II be implemented. The performance obtained from this algorithm should provide a baseline against which any detector (estimator/classifier) can be measured. The generality of the algorithm permits the accomplishment of detailed sensitivity analysis for important system parameters. The performance analysis and sensitivity assessment can be facilitated by the graphical display of the array pattern as discussed in Section III.2.

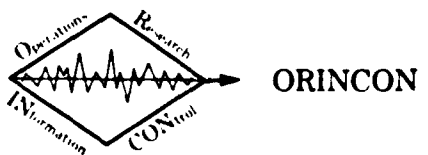
The design and development of the signal processor, based upon the recommended algorithm, should proceed along two complementary paths. On one hand, a simulation should be developed of reasonable sensor outputs. A suitable simulation can be easily defined from the considerations presented in Part I. Then, data can be produced using the simulation that can be used to exercise the signal processing algorithm. By processing simulated data, the performance of the detector/estimator/classifier can be judged by comparing the outputs with "truth." The algorithms can be applied subsequently to data obtained from controlled field experiments. If there are substantial inconsistencies between



the simulated and real data, the simulation should be modified to accord more closely with the physical environment. Thus, the analysis should permit feedback between the artificially-produced data (i.e., simulation) and the experience gained in the field.

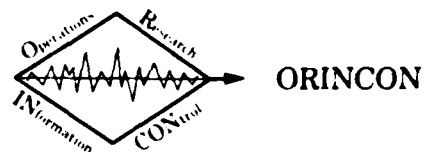
After the performance of the general signal processor has been established, attention should be directed to the assessment of the computational requirements and capability of appropriate algorithms. It is reasonable to expect that limited versions of the general algorithms may be required for implementation in the operational system. An assessment of possible losses in performance must be accomplished during this portion of the effort.

To summarize, this report is intended to provide a perspective on the physical problem that should be used to guide the design and development of the signal processor for a seismic surveillance system. Important physical considerations are discussed in Part I. In Part II, array processing is reviewed and general adaptive array processing algorithms are developed. A unification of physical considerations and signal processing algorithm design is presented in this concluding part of the report.

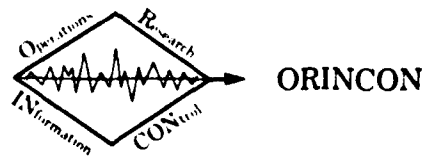


REFERENCES

1. M. B. Dobrin, Introduction to Geophysical Prospecting, 3rd ed., New York: McGraw-Hill, 1976.
2. F. S. Grant and G. F. West, Interpretation Theory in Applied Geophysics, New York: McGraw-Hill, 1965.
3. D. S. ParASNIS, Principles of Applied Geophysics, 3rd ed., A. Halsted Press Book, New York: John Wiley, 1979.
4. W. M. Telford, L. P. Geldart, R. E. Sheriff, and D. A. Keys, Applied Geophysics, Cambridge: Cambridge University Press, 1977.
5. K. Aki and P. Richards, Quantitative Seismology, Volumes I and II, San Francisco, Freeman Publishing, 1980.
6. B. D. Steinberg, Principles of Aperture and Array System Design, Wiley, New York.
7. M. T. Ma, Theory and Application of Antenna Arrays, Wiley, New York, 1974.
8. R. A. Monzingo and T. W. Miller, Introduction to Adaptive Arrays, Wiley, New York, 1980.
9. F. R. Gantmacher, The Theory of Matrices, vol. I, Chelsea Publ. Co., New York, 1960.
10. D. K. Cheng, "Optimization Techniques for Antenna Arrays," IEEE Proceedings, 59, Dec. 1971, pp. 1664-1674.
11. H. W. Sorenson, Parameter Estimation: Principles and Problems, Marcel Dekker Publ. Co., New York, 1980.
12. I. S. Reed, J. D. Mallett, and L. E. Brennan, "Rapid Convergence Rate in Adaptive Arrays," IEEE Trans. on Aero. and Elect. Sys., AES-10, November 1974, pp. 853-863.
13. H. W. Sorenson, "Tutorial Discussion of Statistical Hypothesis Testing," TOR-0074(4409-01)-18, Aerospace Corporation Technical Report, August 1973.
14. C. A. Baird and C. L. Zahm, "Performance Criteria for Narrow-band Array Processing," 1971 IEEE Conf. on Dec. and Control, Dec. 1971, pp. 564-565.



15. W. F. Gabriel, "Adaptive Arrays--An Introduction," Proc. IEEE, 64, Feb. 1976, pp. 239-272.
16. S. Zohar, "Toeplitz Matrix Inversion: The Algorithm of W. F. French," J. Assoc. Comp. Mach., 16, October 1969, pp. 592-601.
17. E. A. Robinson and M. T. Silva, Digital Foundations of Time Series Analysis: Vol. 2, Wave Equation Space-Time Processing, Holden-Day, San Francisco, 1981.



FILMED

